ARTICLES
https://doi.org/10.1038/s42255-018-0004-9
nature metabolism

The long noncoding RNA CHROME regulates cholesterol homeostasis in primates

Elizabeth J. Hennessy[1,13], Coen van Solingen[1,13], Kaitlyn R. Scacalossi[1], Mireille Ouimet[1], Milessa S. Afonso[1], Jurrien Prins[2], Graeme J. Koelwyn[1], Monika Sharma[1], Bhama Ramkhelawon[1], Susan Carpenter[3], Albert Busch[4,5], Ekaterina Chernogubova[4], Ljubica Perisic Matic[4], Ulf Hedin[4], Lars Maegdefessel[4,5], Brian E. Caffrey[6], Maryem A. Hussein[7], Emiliano P. Ricci[8], Ryan E. Temel[9], Michael J. Garabedian[7], Jeffrey S. Berger[1], Kasey C. Vickers[10], Matthew Kanke[11], Praveen Sethupathy[11], Daniel Teupser[12], Lesca M. Holdt[12] and Kathryn J. Moore[1*]

The human genome encodes thousands of long noncoding RNAs (lncRNAs), the majority of which are poorly conserved and uncharacterized. Here we identify a primate-specific lncRNA (CHROME), which is elevated in the plasma and atherosclerotic plaques of individuals with coronary artery disease, and regulates cellular and systemic cholesterol homeostasis. Expression of the lncRNA CHROME is influenced by dietary and cellular cholesterol through the sterol-activated liver X receptor transcription factors, which control genes that mediate responses to cholesterol overload. Using gain- and loss-of-function approaches, we show that CHROME promotes cholesterol efflux and high-density lipoprotein (HDL) biogenesis by curbing the actions of a set of functionally related microRNAs that repress genes in those pathways. CHROME knockdown in human hepatocytes and macrophages increases the levels of miR-27b, miR-33a, miR-33b and miR-128, thereby reducing the expression of their overlapping target gene networks and associated biological functions. In particular, cells that lack CHROME show reduced expression of ABCA1, which regulates cholesterol efflux and nascent HDL particle formation. Collectively, our findings identify CHROME as a central component of the noncoding RNA circuitry that controls cholesterol homeostasis in humans.

The maintenance of cholesterol homeostasis is essential to human health, and its dysregulation results in disease states, including atherosclerotic cardiovascular disease[1]. The removal of excess cholesterol from cells and its delivery to the liver through HDL is important for the prevention of pathological deposition of cholesterol in tissues, in particular in the artery wall, where atherosclerotic plaques form[2]. Understanding the regulatory circuits that contribute to the dynamic and temporal balancing of cholesterol at the cellular and organismal level are thus of critical importance. At the transcriptional level, the sterol-activated liver X receptors (LXRs) have been shown to have key roles in the regulation of genes that control the response to cholesterol excess, particularly the cholesterol transporter ABCA1, which mediates cholesterol efflux and HDL biogenesis[3]. In addition, recent studies have shown that multiple classes of noncoding RNAs, including microRNAs (miRNAs), small nucleolar RNAs and lncRNAs possess regulatory functions that feed into the previously described networks that control cellular lipid metabolism[4–6].

Among the noncoding RNAs, miRNAs have emerged as potent regulators of cholesterol homeostasis through their ability to repress the expression of genes in the integrated pathways of cholesterol and fatty-acid biosynthesis, reverse cholesterol transport and lipid storage[6]. One of the first such miRNAs to be identified was miR-33 (mmu-miR-33-5p in mice; hsa-miR-33a-5p and hsa-miR-33b-5p in humans), which was shown to reduce cholesterol efflux and reverse cholesterol transport by targeting genes that are involved in cholesterol export (for example, *ABCA1*)[7,8], intracellular trafficking (for example, *NPC1*, *OSBPL6* and *ATG5*)[8,9] and bile secretion (for example, *ATP8B1* and *ABCB11*)[10]. The identification of miR-27b and miR-144 as additional repressors of genes that regulate cholesterol efflux (for example, *ABCA1* and *OSBPL6*)[9,11–14], and the demonstration that delivery of modified oligonucleotide inhibitors of miR-33 and miR-144 in mice can increase plasma levels of HDL cholesterol (HDL-C), has underscored the importance of miRNAs as post-transcriptional regulators of cellular and systemic cholesterol homeostasis. Indeed, the relevance of this mechanism in regulating cholesterol metabolism in humans is supported by genome-wide association studies that have uncovered variants in miRNA loci that are associated with abnormal lipoprotein levels and cardiometabolic disease risk[15]. One such example is miR-128, which has been shown to target *ABCA1* and *LDLR* and therefore to regulate plasma levels of HDL and low-density lipoprotein (LDL) cholesterol, respectively[15].

[1]Department of Medicine, Leon H. Charney Division of Cardiology, New York University School of Medicine, New York, NY, USA. [2]Department of Internal Medicine (Nephrology), Einthoven Laboratory for Vascular and Regenerative Medicine, Leiden University Medical Center, Leiden, the Netherlands. [3]Department of Molecular, Cell and Developmental Biology, University of California, Santa Cruz, Santa Cruz, CA, USA. [4]Department of Molecular Medicine and Surgery, Karolinska Institute, Stockholm, Sweden. [5]Department of Vascular and Endovascular Surgery, Klinikum Rechts der Isar, Technical University Munich, Munich, Germany. [6]Max Planck Institute for Molecular Genetics, Berlin, Germany. [7]Department of Microbiology, New York University School of Medicine, New York, NY, USA. [8]INSERM U1111, Centre International de Recherche en Infectiologie, Ecole Normale Supérieure de Lyon, Université de Lyon, Lyon, France. [9]Saha Cardiovascular Research Center, University of Kentucky, Lexington, KY, USA. [10]Department of Medicine, Vanderbilt University Medical Center, Nashville, TN, USA. [11]Department of Biomedical Sciences, College of Veterinary Medicine, Cornell University, Ithaca, NY, USA. [12]Institute of Laboratory Medicine, Ludwig-Maximilians-University Munich, Munich, Germany. [13]These authors contributed equally: E. J. Hennessy, C. v. Solingen. *e-mail: kathryn.moore@nyumc.org

However, given the redundancy in miRNA targeting of the cholesterol efflux pathways described above, it remains unclear whether such functionally related miRNAs are coordinately controlled or regulated by higher-order systems.

lncRNAs contribute to regulatory complexity in higher eukaryotes through diverse mechanisms, including by regulating chromosomal architecture, facilitating the formation of ribonucleoprotein complexes, altering the epigenetic landscape of the genome and mediating transcriptional and post-transcriptional gene regulation[16]. lncRNAs are broadly defined as non-protein-coding RNA transcripts of greater than 200 nucleotides, and they can execute their functions by forming lncRNA–DNA, lncRNA–protein and lncRNA–RNA interactions in the nucleus and/or cytoplasm. Although it is estimated that the human genome contains more than 10,000 lncRNAs, fewer than 5% of human lncRNAs have been functionally characterized, in part because poor conservation among species has hindered their investigation[17,18]. Functional roles for lncRNAs in regulating cholesterol metabolism and cardiovascular disease are beginning to emerge[5,19]. For example, several lncRNAs have been identified that promote or inhibit the function of the sterol response element–binding protein (SREBP) transcription factors, which regulate genes involved in cholesterol and fatty-acid synthesis, including MALAT1 (ref. [20]), H19 (ref. [21]), lncHR1 (ref. [22]) and LeXis[23]. Other lncRNAs, such as MeXis[24], have been shown to induce cell-type-specific expression of genes (for example, *ABCA1*) by regulating the chromosomal architecture. Notably, the majority of cardiovascular disease–associated sequence variants that have been identified by human genome-wide association studies are found in the noncoding landscape of the genome, including the locus on chromosome 9p21, which contains the lncRNA ANRIL[25,26], which has the highest association with risk of atherosclerosis and cardiovascular events. Understanding the functional importance of noncoding RNAs that contribute to disease remains a major challenge.

Here we describe a primate-specific lncRNA, which is increased in the setting of human atherosclerotic vascular disease and contributes to the maintenance of cholesterol homeostasis. Studies in nonhuman primates show that expression of the lncRNA CHROME is upregulated in response to a cholesterol-enriched diet and by activation of the LXR transcription factors that coordinate the response to cholesterol excess. Using loss- and gain-of-function studies, we establish that CHROME increases the efflux of excess cholesterol from cells and promotes hepatic HDL biogenesis by curbing the actions of a set of miRNAs, which share the ability to repress genes that are involved in cholesterol efflux and reverse cholesterol transport. In agreement with these mechanistic studies, we find that hepatic levels of CHROME are inversely correlated with those of its miRNA targets and positively correlated with plasma levels of HDL-C in a human cohort. In summary, our identification of CHROME unveils the regulatory cross-talk between noncoding RNAs that sustains cholesterol homeostasis in humans in health and disease.

Results

CHROME is a primate-specific lncRNA increased in atherosclerotic vascular disease. The lncRNA AC009948.5 (ENSG00000223960), which we have named CHROME (for cholesterol homeostasis regulator of miRNA expression), is proximal to a locus on human chromosome 2 that is linked to premature coronary artery disease[27] and plasma HDL-C levels[28]. The *CHROME* locus contains primate-specific Alu transposable repeat elements[29], and *CHROME* exons are conserved in the genomes of primates but are largely absent from the genomes of other placental mammals or vertebrates (Fig. 1a and Supplementary Fig. 1a–c). We identified seven splice variants of CHROME (Fig. 1a) that are broadly expressed in human tissues and cell types (Supplementary Fig. 2a–c). To test whether CHROME expression is altered in the setting of atherosclerotic vascular disease, we measured its expression in the plasma and arteries of individuals with coronary artery disease and healthy control subjects. Plasma levels of CHROME, measured by quantitative PCR (qPCR) using primers directed to a common region in all variants, were found to be markedly higher in individuals with coronary artery disease than in healthy individuals (Fig. 1b), whereas the expression levels of LIPCAR and TapSAKI (other known circulating lncRNAs) remained unchanged (Supplementary Fig. 3a). Furthermore, analysis of CHROME expression in the Biobank of Karolinska Endarterectomies (BiKE) Affymetrix microarray datasets[30] showed that CHROME RNA levels were increased in atherosclerotic plaques from patients with symptomatic and asymptomatic carotid stenosis compared with control arterial samples (Fig. 1c). This was confirmed by qPCR for individual CHROME variants by using exon-spanning primers complementary to unique sequences present in each of the CHROME isoforms (Supplementary Fig. 3b). To understand the cellular distribution of CHROME in the healthy and diseased artery wall, we performed RNA in situ hybridization. We found that in carotid artery plaques, CHROME RNA was localized to infiltrating inflammatory cells in both the neointima and areas of plaque rupture (Fig. 1d and Supplementary Fig. 3c). In contrast, there was little detectable CHROME RNA in the normal artery wall (Fig. 1e and Supplementary Fig. 3d). Together, these data suggest a potential function for CHROME in the setting of atherosclerotic vascular disease.

CHROME is upregulated in response to excess dietary or cellular cholesterol through LXR. To test whether CHROME expression is responsive to dietary and cellular cholesterol levels, we measured its expression in the livers of nonhuman primates before and after feeding the animals a diet enriched in cholesterol for 8 weeks. We observed that increasing the dietary cholesterol levels increased the expression of CHROME-1, CHROME-3 and CHROME-7 in the liver—a tissue that is critical for the regulation of systemic cholesterol homeostasis—compared with the low-fat chow diet (Fig. 2a). We found that CHROME was abundantly expressed in primary human hepatocytes (10^2 copies per cell; Supplementary Fig. 4a), and levels of CHROME variants increased with cyclodextrin–cholesterol treatment compared with vehicle treatment (Fig. 2b). In addition to hepatocytes, macrophages have key roles in cholesterol homeostasis, particularly in the atherosclerotic plaque, where they are recruited to clear accumulated LDL[31]. In human THP-1 monocytic cells that were differentiated into macrophages in vitro, CHROME was present at more than 10^2 copies per cell (Supplementary Fig. 4a), and its expression levels increased on cholesterol loading with acetylated LDL (Fig. 2c). Using prediction algorithms to uncover potential transcriptional regulators of CHROME, we identified putative binding sites for the sterol-activated LXR transcription factors (Supplementary Fig. 4b), which coordinate the expression of genes involved in cellular and systemic responses to cholesterol excess[3]. We performed chromatin immunoprecipitation in THP-1 macrophages treated with a LXR agonist and observed LXR occupancy at the *CHROME* locus, at sites upstream of the transcription start site and within the first intron (Fig. 2d). The levels of LXR enrichment over IgG control at these two sites in the *CHROME* locus were similar in magnitude to those found for the known LXR-responsive gene *OSBPL6*, which served as a positive control (Fig. 2d). In agreement with a role for LXR in regulating CHROME transcription, treatment of nonhuman primates with the LXR agonist GW3965 increased levels of CHROME-1, CHROME-3, CHROME-4 and CHROME-7 in the liver, relative to control vehicle treatment (Fig. 2e). Furthermore, treatment of primary human hepatocytes, HepG2 cells and THP-1 macrophages with the LXR agonist T0901317, compared with vehicle treatment, increased the expression of CHROME variants (Fig. 2f and Supplementary Fig. 4c). Notably,

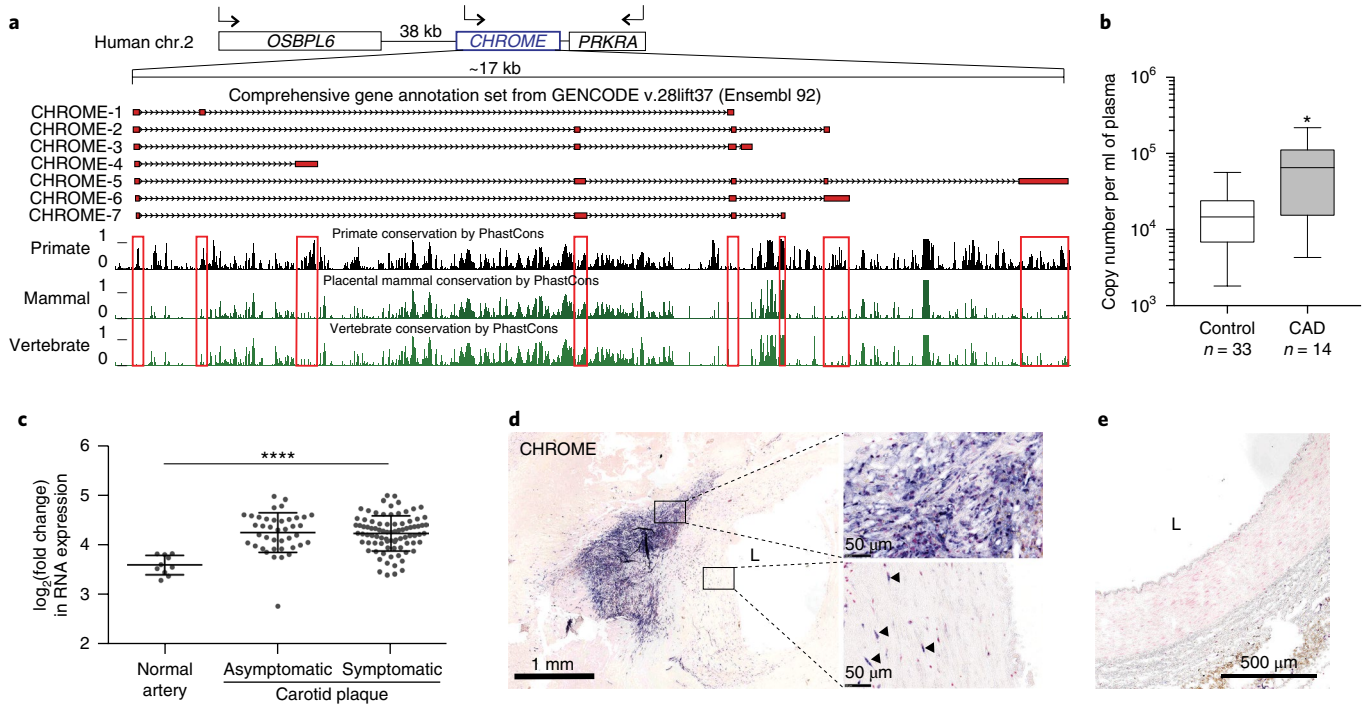

Fig. 1 | Levels of lncRNA CHROME are increased in atherosclerotic cardiovascular disease. a, Schematic representation of the human *CHROME* locus, which encodes seven splice variants (CHROME-1–CHROME-7). PhastCons analysis showing the conservation of *CHROME* in primates but not in other mammals or vertebrates. Red boxes indicate exonic sequences. Primates include chimpanzee, rhesus and bushbaby. Mammals include tree shrew, mouse, rat, guinea pig, rabbit, shrew, hedgehog, dog, cat, horse, crow, armadillo, elephant and tenrec. Vertebrates include, opossum, platypus, lizard, chicken, *Xenopus tropicalis*, zebrafish, tetrdon, fugu, stickleback and medaka. **b**, Box and whiskers plot depicting plasma levels of CHROME RNA in individuals with coronary artery disease (CAD, $n=14$) or healthy control subjects ($n=33$). Box represents 25th to 75th percentiles and the middle line indicates the median. **c**, CHROME expression in normal artery ($n=10$) or carotid endarterectomy plaques from individuals with asymptomatic ($n=40$) or symptomatic ($n=77$) carotid stenosis. Data are the mean ± s.e.m. **d**,**e**, Detection of CHROME RNA (purple) by in situ hybridization of human carotid plaque (**d**) and control iliac artery (**e**). Sections were counterstained with nuclear fast red to visualize nuclei (pink). Boxed regions in **d** indicate CHROME expression in areas of inflammatory cell infiltrate (top) and in the neointima (bottom, arrowheads). L, lumen. Data are representative of staining from eight independent plaques. *P* values were calculated using a Mann–Whitney *U*-test (**b**) or two-way analysis of variance (ANOVA) (**c**); $^{*}P \leq 0.05$, $^{****}P \leq 0.0001$.

treatment with T0901317 or acetylated LDL did not increase expression of CHROME or the control gene *ABCA1* in THP-1 macrophages when LXRα and/or LXRβ were silenced with short interfering RNAs (siRNAs) (Fig. 2g and Supplementary Fig. 4d). Together, these data identify *CHROME* as part of the network of genes that are regulated by LXR in primates in the settings of excess dietary or cellular cholesterol.

CHROME knockdown in hepatocytes reveals roles in cholesterol metabolism. To determine the function of CHROME, we first examined its subcellular distribution pattern, as this can provide insight into the potential biological role of a lncRNA[32]. Using fluorescence in situ hybridization (FISH), we found that CHROME transcripts were distributed both in the nucleus and the cytoplasm in HEK293T cells (Fig. 3a), THP-1 macrophages (Supplementary Fig. 4e) and HepG2 cells (data not shown). The finding that CHROME was localized in the cytoplasm, the site of RNA translation, raised the possibility that it might contain an actively translated open reading frame. However, coding-potential and Kozak-sequence-prediction algorithms indicated that CHROME had a low coding potential (Supplementary Fig. 5a,b and Supplementary Table 1), as confirmed by polysome fractionation in THP-1 macrophages (Supplementary Fig. 5c,d). To test the effect of CHROME loss of function, we used short hairpin RNAs (shRNAs), which preferentially deplete cytoplasmic lncRNAs[33], to target a region in exon 1 that all CHROME variants have in common (Supplementary Fig. 6a). Using lentiviral delivery of control and CHROME-targeting shRNAs, we generated human hepatic HepG2 cell lines in which CHROME variants were constitutively knocked down (Fig. 3b), and performed RNA sequencing (RNA-seq). Ingenuity pathway analysis of the RNA-seq datasets identified lipid metabolism functions as among the top canonical pathways altered on CHROME knockdown in HepG2 cells (Fig. 3c), most notably, the LXR pathway, which regulates cellular responses to excess cholesterol, the farnesoid X receptor (FXR) pathway, whih regulates bile acid metabolism and cholesterol excretion, and the fatty-acid β-oxidation pathway (Fig. 3c and Supplementary Fig. 6b,c).

CHROME post-transcriptionally regulates ABCA1 expression and cholesterol efflux. Activation of LXRs promotes cholesterol homeostasis through induction of a cadre of genes involved in cellular cholesterol efflux and reverse cholesterol transport. To investigate the role of CHROME in LXR-mediated responses, we measured the ability of HepG2 cells that expressed control or CHROME-targeting shRNAs to efflux cholesterol to apolipoprotein A1 (APOA1), a process central to HDL biogenesis in the liver. Cholesterol efflux to exogenously supplied APOA1 was 50% lower in HepG2 cells expressing *CHROME* shRNAs than control shRNAs (Fig. 3d). To confirm our findings, we used a second method of CHROME depletion in primary human hepatocytes, in which we acutely knocked down CHROME by transfecting GapmeR antisense oligonucleotides that target a region in exon 1, which all variants have in common (Fig. 3e). In agreement with our findings using shRNAs, CHROME depletion in primary human hepatocytes with GapmeR

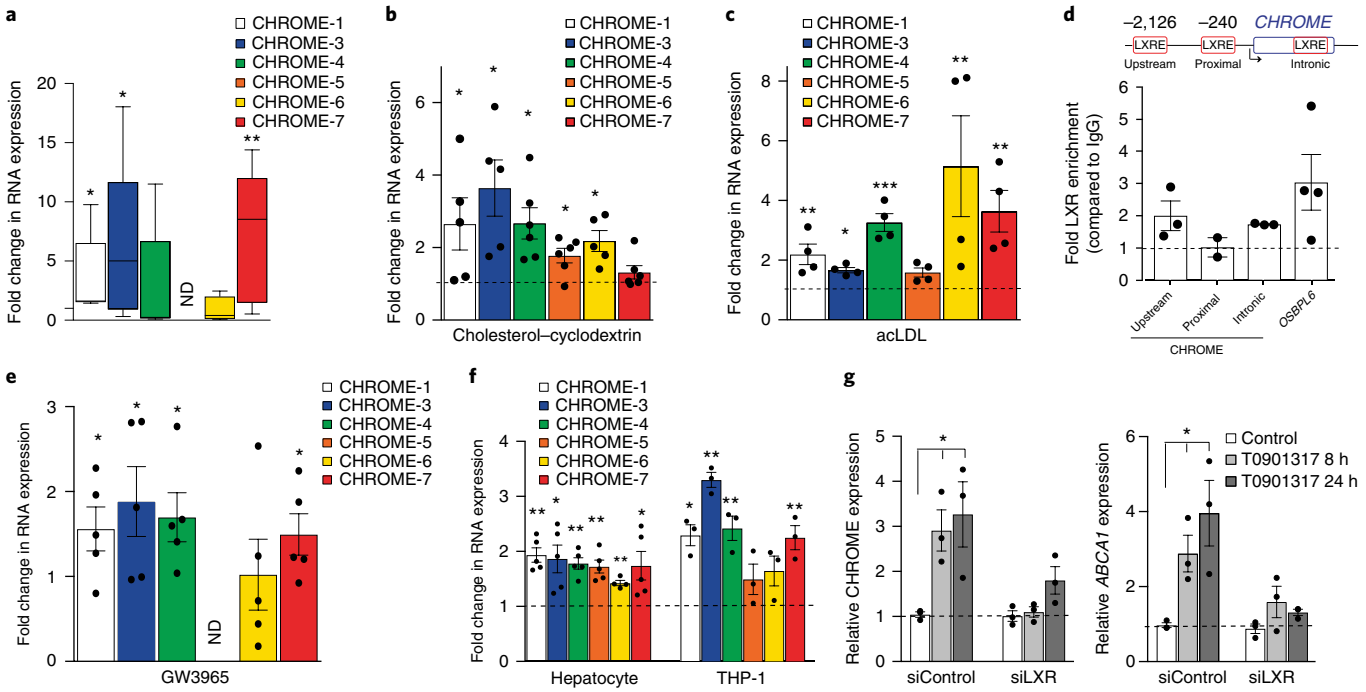

Fig. 2 | The lncRNA CHROME is regulated by dietary and cellular cholesterol by LXR transcription factors. a, qPCR analysis of CHROME variant expression in livers of African green monkeys ($n=5$ per group) fed a high-fat moderate-cholesterol diet (8 weeks) compared with a baseline chow diet. Box represents twenty-fifth to seventy-fifth percentiles; middle line indicates the median. ND, not detected. **b**,**c**, qPCR analysis of CHROME variant expression in human HepG2 cells treated with cholesterol–cyclodextrin (10 μg ml^{-1}; 72 h) compared with vehicle (**b**) and human THP-1 macrophages treated with acetylated LDL (acLDL; 37.5 μg ml^{-1}, 24 h) compared with untreated cells (**c**). Data are the mean ± s.e.m. of five (**b**) or four (**c**) independent experiments. **d**, Schematic diagram of predicted LXR response elements (LXRE) in the *CHROME* locus (top) and relative enrichment of CHROME in LXRα/β chromatin immunoprecipitates from THP-1 cells treated with a LXR agonist (T0901317, 10 μM) at each of the predicted sites. Enrichment of LXR at the *OSBPL6* locus is shown as a positive control. Data are normalized to IgG control. **e**, qPCR analysis of CHROME variant expression in livers of male cynomolgus monkeys treated with LXR agonist (GW3965) or vehicle for 2 d. Data are the mean ± s.e.m. of five monkeys per group. **f**, qPCR analysis of CHROME variant expression in primary human hepatocytes and THP-1 macrophages treated with a LXR agonist (10 μM T0901317) relative to vehicle control. Data are the mean ± s.e.m. of 3–5 independent experiments. **g**, qPCR quantification of CHROME (all variants) and *ABCA1* mRNA in THP-1 macrophages transfected with an LXRα- and LXRβ-targeting (siLXR) or control siRNA (siControl) for 24 h and then treated with LXR agonist (10 μM T0901317). Data are the mean ± s.e.m. of three biological replicates from a single experiment that is representative of three experiments. *P* values were calculated using a two-tailed Student's *t*-test (**b**,**c**,**f**,**g**) or two-way ANOVA (**a**,**e**). $^*P \le 0.05$, $^{**}P \le 0.01$, $^{***}P \le 0.001$.

oligonucleotides lowered cholesterol efflux to exogenous APOA1 by approximately 50% compared with control GapmeR treatment (Fig. 3f). We next measured the effects of CHROME on nascent HDL formation by primary human hepatocytes, by using ^{14}C-choline to label de novo synthesized phospholipids. Immunoprecipitation of APOA1 secreted by primary human hepatocytes revealed 50% lower levels of APOA1 lipidation in cells teated with GapmeR oligonucleotides against CHROME compared with GapmeR-control-treated cells (Fig. 3g). In contrast, CHROME knockdown or overexpression in HepG2 cells did not alter the expression of genes involved in LDL uptake or cholesterol synthesis, nor were these processes altered on manipulation of CHROME levels (Supplementary Fig. 7a–e). Because the ABCA1 transporter regulates cholesterol and phospholipid efflux to APOA1, we next measured the effect of CHROME knockdown on ABCA1 protein and mRNA levels. We observed lower ABCA1 protein expression in hepatocytes treated with GapmeR oligonucleotides against CHROME than in GapmeR-control-treated hepatocytes (Fig. 3h and Supplementary Fig. 7f). Using PCR primers to differentiate between mature and unspliced mRNA transcripts[34] of *ABCA1*, we found that CHROME depletion reduced the levels of mature, but not nascent, *ABCA1* mRNA (Fig. 3i), suggesting a post-transcriptional mechanism.

CHROME localizes to processing bodies and associates with miRNAs. The cytoplasmic localization of CHROME raised the possibility that it might interact with cytosolic miRNAs that are known to post-transcriptionally regulate *ABCA1* expression and cholesterol efflux. To explore this potential mechanism, we used the miRTarget2 algorithm, which identified miR-33a, miR-33b, miR-27b and miR-128 to be among the top miRNAs predicted to interact with CHROME (Supplementary Table 2). Using RNA hybrid analysis and manual curation, we found that CHROME variants contain numerous putative binding sites for each of these miRNAs that have experimentally been validated to regulate cholesterol efflux and/or HDL metabolism[8,15,35,36] (Fig. 4a and Supplementary Fig. 8). Using RNAcofold, which takes into account the length and secondary structure of the transcripts, we calculated the free energy changes associated with the formation of CHROME–miRNA complexes and found that it predicted stable interactions of CHROME with miR-27b, miR-33a, miR-33b and miR-128, but not the control miRNA miR-16 (Fig. 4b). To first assess whether CHROME associates with miRNA complexes, we immunoprecipitated AGO2 from primary human hepatocytes and used qPCR to detect associated RNA, focusing on CHROME-1, CHROME-3 and CHROME-7, as these were the variants that were regulated the most by cholesterol in monkeys. We found that CHROME-1, CHROME-3 and CHROME-7 transcripts were enriched in AGO2 immunoprecipitates compared with control IgG precipitates (Fig. 4c). Similar associations between CHROME variants and AGO2 were observed in THP-1 macrophages (Fig. 4c). To test whether CHROME binds

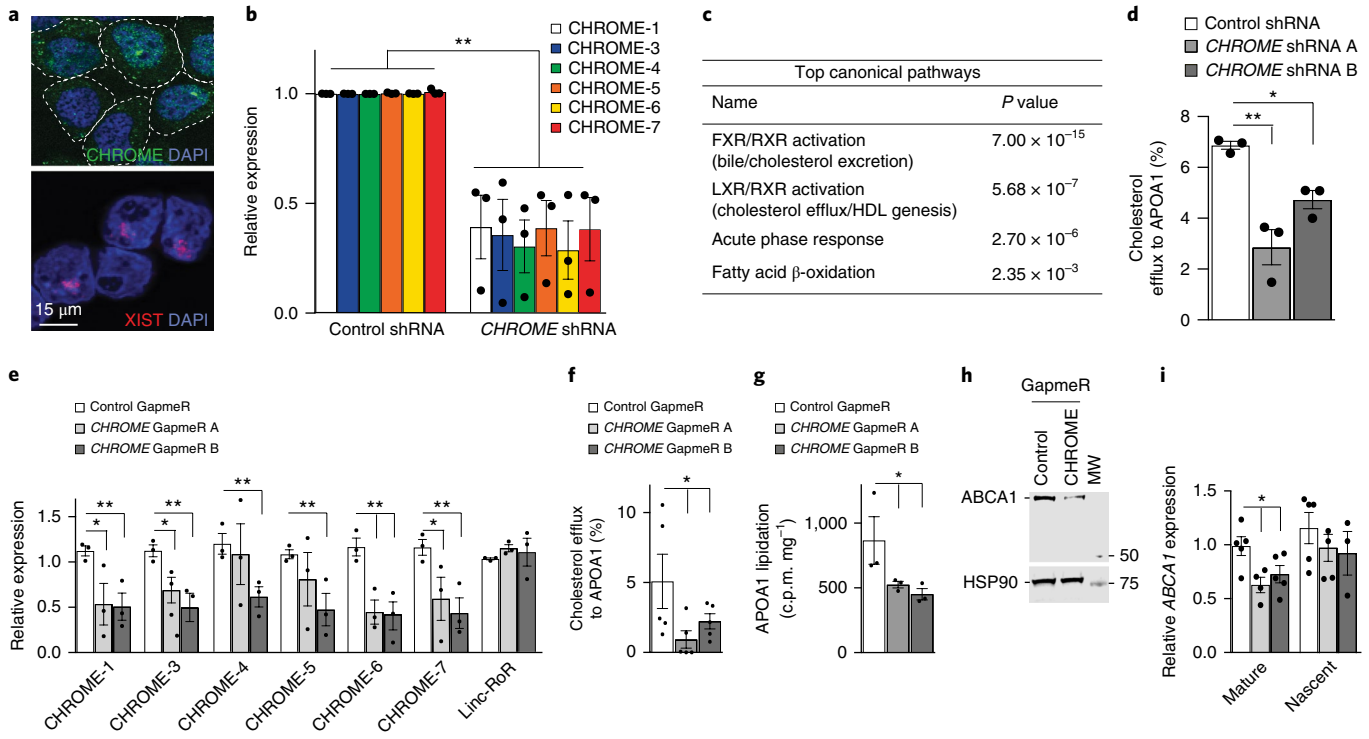

Fig. 3 | CHROME depletion in hepatocytes reduces cholesterol efflux and formation of nascent HDL particles. a, FISH of CHROME (green) and XIST (red) RNA in HEK293T cells stained with DAPI to visualize nuclear DNA (blue). **b**, qPCR analysis of CHROME variants in HepG2 cells stably expressing an shRNA that targets all CHROME variants (*CHROME* shRNA) or control shRNA. **c**, Ingenuity pathway analysis of RNA-seq data from *CHROME* shRNA- and control shRNA-expressing HepG2 cells showing the top canonical pathways that are altered on CHROME knockdown. **d**, Measurement of cholesterol efflux to exogenous APOA1 in HepG2 cells that express *CHROME* or control shRNAs. **e**, qPCR quantification of CHROME variants in primary human hepatocytes transfected with control (control GapmeR) or CHROME-targeting GapmeRs (*CHROME* GapmeR A or *CHROME* GapmeR B). Linc-RoR, long intergenic non-protein-coding RNA, regulator of reprogramming. **f**, Measurement of cholesterol efflux to exogenous APOA1 in primary human hepatocytes transfected with control or CHROME-targeting GapmeRs. **g**, Measurement of phospholipid efflux to APOA1 secreted from primary human hepatocytes labelled with C^{14}-choline chloride and transfected with control or CHROME-targeting GapmeRs. **h**, Western blot analysis of ABCA1 and HSP90 (control) in hepatocytes transfected with control or CHROME-targeting GapmeRs. A molecular weight (MW) marker is shown on the right. **i**, qPCR analysis of mature and nascent *ABCA1* mRNA transcripts in primary human hepatocytes transfected with control or CHROME-targeting GapmeRs. **b**,**d**-**i**, Data are the mean ± s.e.m. of 3–5 independent experiments. *P* values were calculated using a two-tailed Student's *t*-test. $^{*}P \leq 0.05$, $^{**}P \leq 0.01$.

specifically to miR-27b, miR-33a, miR-33b and miR-128, we used MS2-tagged RNA affinity purification (MS2-TRAP)[37]. We cloned CHROME-1, CHROME-3 and CHROME-7 upstream of MS2-binding sequences, and coexpressed these constructs in HEK293T cells with a yellow fluorescent protein (YFP)-tagged MS2-binding protein, which was used as bait to isolate MS2-tagged RNAs. qPCR analysis of RNAs that coprecipitated with CHROME–MS2-binding protein complexes, by using an anti-YFP antibody, showed specific enrichment of miR-27b, miR-33a, miR-33b and miR-128 relative to control IgG, whereas no enrichment of control miRNAs (for example, miR-16, miR-224 and miR-155) was detected (Fig. 4d).

To further investigate the association of CHROME with the RNA-induced silencing complex, we performed RNA FISH for CHROME in HEK293T cells that stably expressed green fluorescent protein (GFP)-tagged AGO2 (AGO2-GFP). We observed colocalization of CHROME and AGO2 in puncta that were present in the cytoplasm (Fig. 4e). Notably, these puncta stained positive for enhancer of mRNA-decapping protein 4 (EDC4) (Fig. 4e), a marker of RNA-processing bodies (P-bodies) that mediate miRNA sequestration or decay[38]. The presence of CHROME in P-bodies was confirmed by querying publicly available RNA-seq data (ArrayExpress accession number E-MTAB-5477) of transcripts isolated from P-bodies that were purified from HEK293T cells through fluorescence-activated particle sorting[39]. CHROME was found to be significantly over-represented in the P-body fraction compared with the non-P-body fraction (adjusted *P* value = 0.03; see ref. [39]). Together, these data suggest that CHROME is localized to P-bodies, where it may sequester or degrade its miRNA binding partners. To investigate this possibility, we performed miRNA-competition experiments with either wild-type CHROME-7 (CHROME-7^{WT}) or a CHROME-7 mutant in which the miRNA-binding sites were mutated (CHROME-7^{MUT}). We transfected HEK293T cells with either CHROME-7^{WT} or CHROME-7^{MUT} and increasing amounts of control, miR-33a, miR-27b or miR-128 mimics. We found that cells expressing CHROME-7^{WT}, but not CHROME-7^{MUT}, had lower levels of miR-33a, miR-27b and miR-128 than did vector-transfected cells. Because we controlled the concentration of miRNA molecules in this experiment by transfection, this result suggests that CHROME can induce the decay of miR-33, miR-27b and miR-128 (Supplementary Fig. 9a).

CHROME modulates the actions of miRNAs known to repress cholesterol efflux and HDL biogenesis. To further investigate whether endogenous CHROME binding of miR-27b, miR-33a, miR-33b and miR-128 reduces the biological activities of these miRNAs, we assessed the effects of CHROME knockdown on the target gene networks of the miRNAs by using two unbiased approaches. First, we analyzed our RNA-seq dataset of genes differentially expressed in HepG2 cells that expressed shRNA against CHROME and control shRNA-expressing HepG2 cells through cumulative distribution function analysis to identify whether mRNAs targeted by miR-33a,

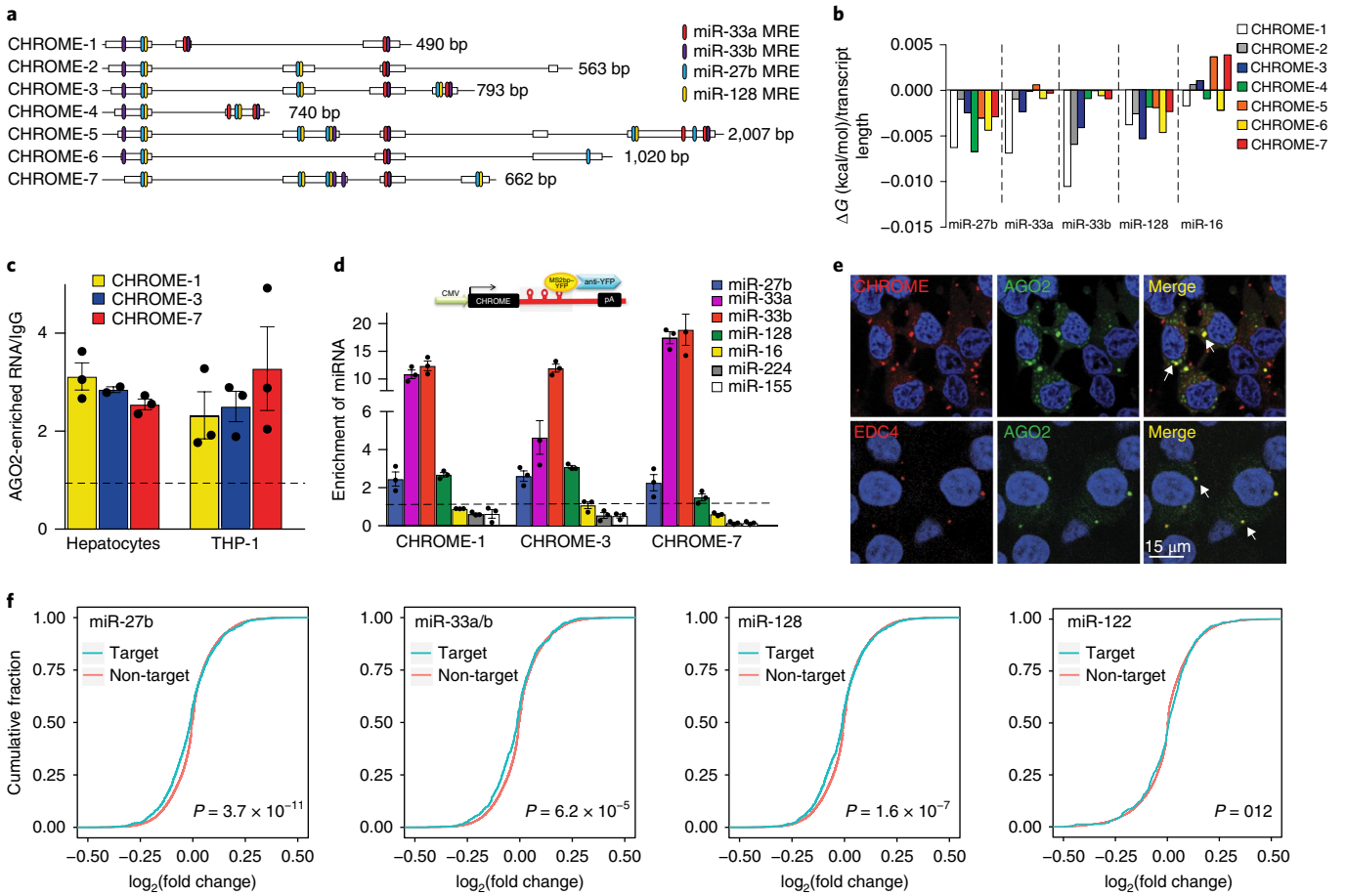

Fig. 4 | CHROME interacts with a set of miRNAs known to repress cholesterol efflux. a, Schematic diagram showing multiple miRNA response elements (MRE) for miR-27b, miR-33a, miR-33b and miR-128 in CHROME variants. **b**, RNAcofold-predicted changes in Gibbs free energy (Δ*G*) upon binding of CHROME variants to miR-27b, miR-33a, miR-33b, miR-128 or miR-16 (control). **c**, Enrichment of CHROME RNA in AGO2 immunoprecipitates from primary human hepatocytes and THP-1 macrophages relative to IgG control. **d**, qPCR detection of miRNAs in CHROME-1, CHROME-3 and CHROME-7 ribonucleoprotein complexes precipitated with MS2-TRAP. Data are normalized to *U6* and control MS2bs-vector. **c**,**d**, Data are the mean ± s.e.m. of a single experiment and are representative of three independent experiments. **e**, FISH of CHROME (red, top) and immunostaining for the P-body marker EDC4 (red, bottom) in HEK293T cells expressing AGO2–GFP (green) and stained with DAPI nuclear stain (blue). Arrows in the merged image indicate signal colocalization (yellow) in punctate structures. Staining is representative of two independent experiments. CMV, cytomegalovirus; pA, polyadenylation; MS2bp, MS2 binding protein. **f**, Cumulative distribution plots of $\log_2$-transformed fold change in gene expression, by using RNA-seq for *CHROME* shRNA- versus control shRNA-expressing HepG2 cells (three biological replicates each), showing genes containing miR-27b, miR-33a/miR-33b or miR-128 target sites predicted by Targetscan (blue) and all other expressed genes (red). As a control, similar analyses were performed for genes containing target sites of miR-122, a hepatic miRNA with known roles in lipid metabolism. The increased prevalence of negative $\log_2$ fold changes among predicted targets of miR-27b, miR-33 and miR-128 (left shift of blue line compared to red), but not miR-122, suggests increased inhibitory effects of those miRNAs on CHROME knockdown. *P* values were calculated using a two-sample Kolmogorov–Smirnov test.

miR-33b, miR-27b and miR-128 were selectively downregulated compared with non-target mRNAs. We found significant overrepresentation of gene expression inhibition among miR-33a, miR-33b, miR-27b and miR-128 targets predicted by Targetscan, compared with non-target mRNAs, as indicated in the cumulative distribution plot by a shift toward negative $\log_2$ fold changes in expression of targets compared to non-targets (Fig. 4f). In contrast, mRNAs predicted to be targeted by miR-122, a control hepatic miRNA with known roles in lipid metabolism, showed no shift in $\log_2$ fold change in expression from non-target mRNAs, among genes differentially expressed in *CHROME* shRNA- and control shRNA-expressing HepG2 cells (Fig. 4f). To validate these findings, we used the bioinformatics tool miRHub to identify miRNAs that might act as regulatory hubs to control the genes differentially expressed in *CHROME* shRNA- and control shRNA-expressing HepG2 cells. miRHub predicts miRNA target sites in the 3′ untranslated regions (UTRs) of differentially expressed genes and then determines by Monte Carlo simulation, for each miRNA, whether the number and strength of predicted targets is significantly greater than expected by chance. Through this unbiased approach, miR-27b and miR-128 were predicted to act as master regulators of genes that are significantly downregulated on CHROME knockdown (Supplementary Fig. 9b), suggesting that the activity of these miRNAs is increased in the absence of CHROME.

To experimentally test whether CHROME could alter cellular levels of its miRNA-binding partners (miR-27b, miR-33a, miR-33b and miR-128) and their target mRNAs, we performed knockdown and overexpression experiments in hepatocytes. In primary human hepatocytes and HepG2 cells in which CHROME was depleted by using GapmeRs (Fig. 5a) or shRNA (Supplementary Fig. 9c), respectively, the levels of miR-27b, miR-33a, miR-33b and miR-128 were higher than those in cells treated with control GapmerRs or shRNAs. In contrast, no differences in levels of the control miRNA miR-16 were observed in cells treated with

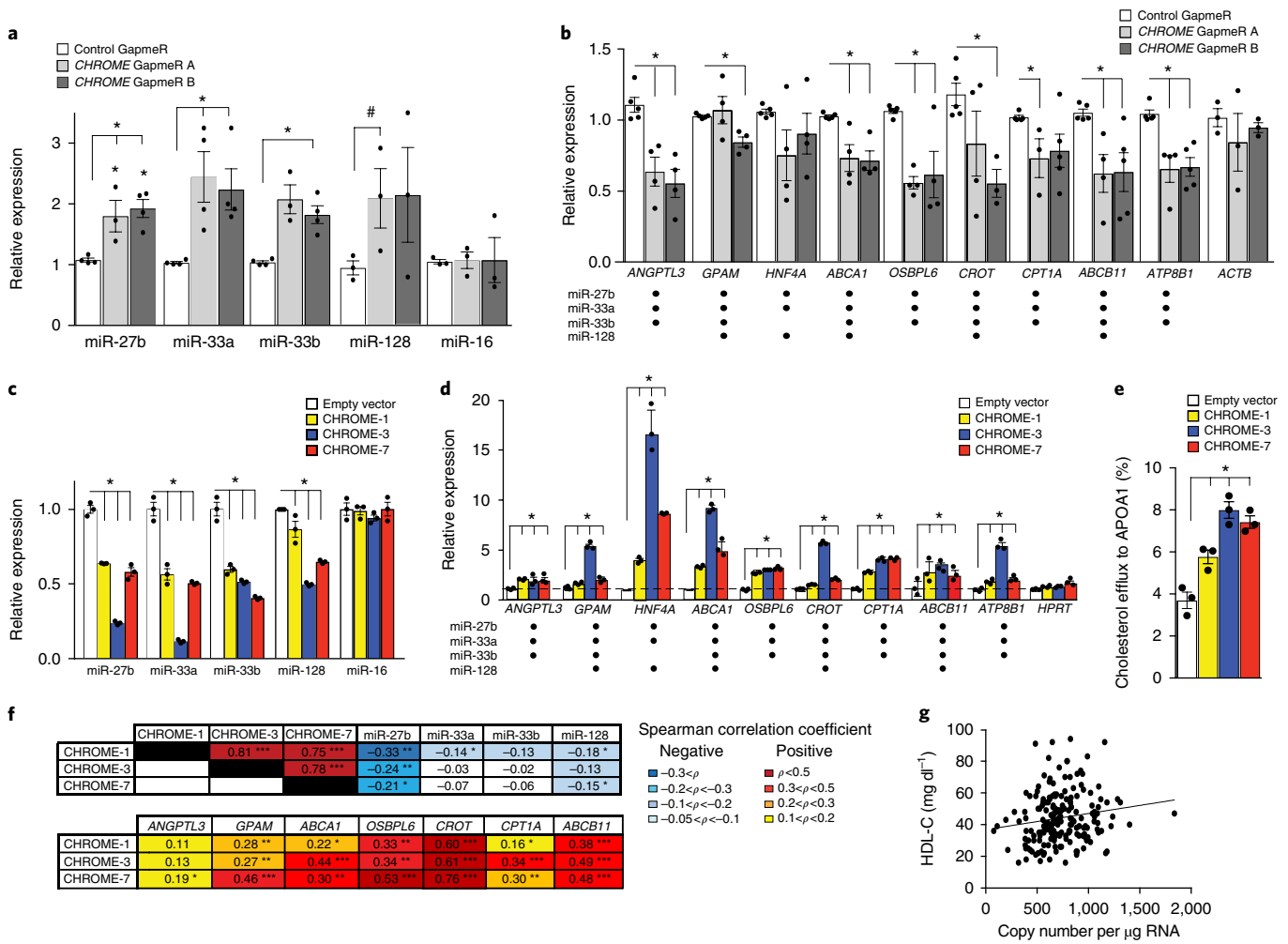

	CHROME-1	CHROME-3	CHROME-7	miR-27b	miR-33a	miR-33b	miR-128
CHROME-1		0.81 ***	0.75 ***	−0.33 **	−0.14 *	−0.13	−0.18 *
CHROME-3			0.78 ***	−0.24 **	−0.03	−0.02	−0.13
CHROME-7				−0.21 *	−0.07	−0.06	−0.15 *

	ANGPTL3	*GPAM*	*ABCA1*	*OSBPL6*	*CROT*	*CPT1A*	*ABCB11*
CHROME-1	0.11	0.28 **	0.22 *	0.33 **	0.60 ***	0.16 *	0.38 ***
CHROME-3	0.13	0.27 **	0.44 ***	0.34 **	0.61 ***	0.34 ***	0.49 ***
CHROME-7	0.19 *	0.46 ***	0.30 **	0.53 ***	0.76 ***	0.30 **	0.48 ***

Fig. 5 | Gain or loss of CHROME in hepatocytes alters levels of its interacting miRNAs and their common target mRNAs involved in cholesterol metabolism. a-**d**, qPCR analysis of levels of miRNAs (**a**,**c**) and their common target mRNAs (**b**,**d**) in primary human hepatocytes transfected with control (control GapmeR) or CHROME-targeting GapmeRs (*CHROME* GapmeR A or B) (**a**,**b**) or HepG2 cells stably expressing CHROME-1, CHROME-3, CHROME-7 or empty vector (**c**,**d**). **b**,**d** Table shows validated targets of miR-27b, miR-33a, miR-33b and miR-128. **e**, Measurement of cholesterol efflux to exogenous APOA1 in THP-1 macrophages stably expressing empty vector, CHROME-1, CHROME-3 or CHROME-7. **f**, Spearman rank correlation coefficients (ρ) of CHROME RNA copy number with its interacting miRNAs and their target mRNAs in human liver ($n = 200$). **g**, Scatter plot showing the relationship between hepatic CHROME-7 copy number and plasma levels of HDL cholesterol ($n = 200$). Spearman correlation coefficients between CHROME-7 copy number and plasma levels of HDL cholesterol ($n = 200$, $\rho = 0.1722$, $P = 0.0019$) were calculated using SAS statistic software. **a**–**e**, Data are the mean ± s.e.m. of three independent experiments, and *P* values were calculated using a two-tailed Student's *t*-test. #$P \leq 0.1$, *$P \leq 0.05$, **$P \leq 0.001$, ***$P \leq 0.000001$.

control and CHROME-targeting GapmeRs or shRNAs (Fig. 5a, Supplementary Fig. 9c). In agreement with the increased levels of miR-27b, miR-33a, miR-33b and miR-128, we observed reduced levels of their common mRNA targets on CHROME depletion by GapmeRs in primary human hepatocytes (Fig. 5b) or shRNA in HepG2 cells (Supplementary Fig. 9d), as compared with control treatments. In contrast, we observed no difference in the mRNA levels of the control gene *ACTB* (Fig. 5b), or *PRKRA*, the gene adjacent to *CHROME* (Supplementary Data Fig. 9e). Conversely, overexpression of CHROME-1, CHROME-3 or CHROME-7 by retroviral transduction of HepG2 cells reduced the levels of miR-27b, miR-33a, miR-33b and miR-128 (Fig. 5c) and increased mRNA levels of their common target genes (Fig. 5d), as compared with those in control vector-expressing HepG2 cells. In agreement with the shared ability of CHROME-targeted miRNAs to repress cholesterol efflux, we observed an increase in key genes in this pathway, including *ABCA1* and *OSBPL6* (Fig. 5d), and twofold higher levels of cholesterol efflux to APOA1 (Fig. 5e), when CHROME was overexpressed in HepG2 cells, as compared with the control vector. No change in expression of *PRKRA*, the gene adjacent to *CHROME*, was observed when CHROME was overexpressed (Supplementary Fig. 9f).

To further investigate the relationship of CHROME with its miRNA binding partners and their target genes in humans, we obtained healthy hepatic tissue from 200 patients undergoing liver surgery and measured RNA levels by qPCR. In agreement with our in vitro findings, we found that levels of CHROME in the liver were inversely correlated with levels of miR-27b, miR-33a, miR-33b and miR-128, and positively correlated with levels of their target mRNAs (Fig. 5f). Furthermore, in accordance with a role for CHROME in regulating hepatic cholesterol efflux to APOA1, we found that hepatic expression of CHROME-7 was positively and significantly correlated with plasma levels of HDL-C (Fig. 5g) and APOA1 (Supplementary Fig. 9g).

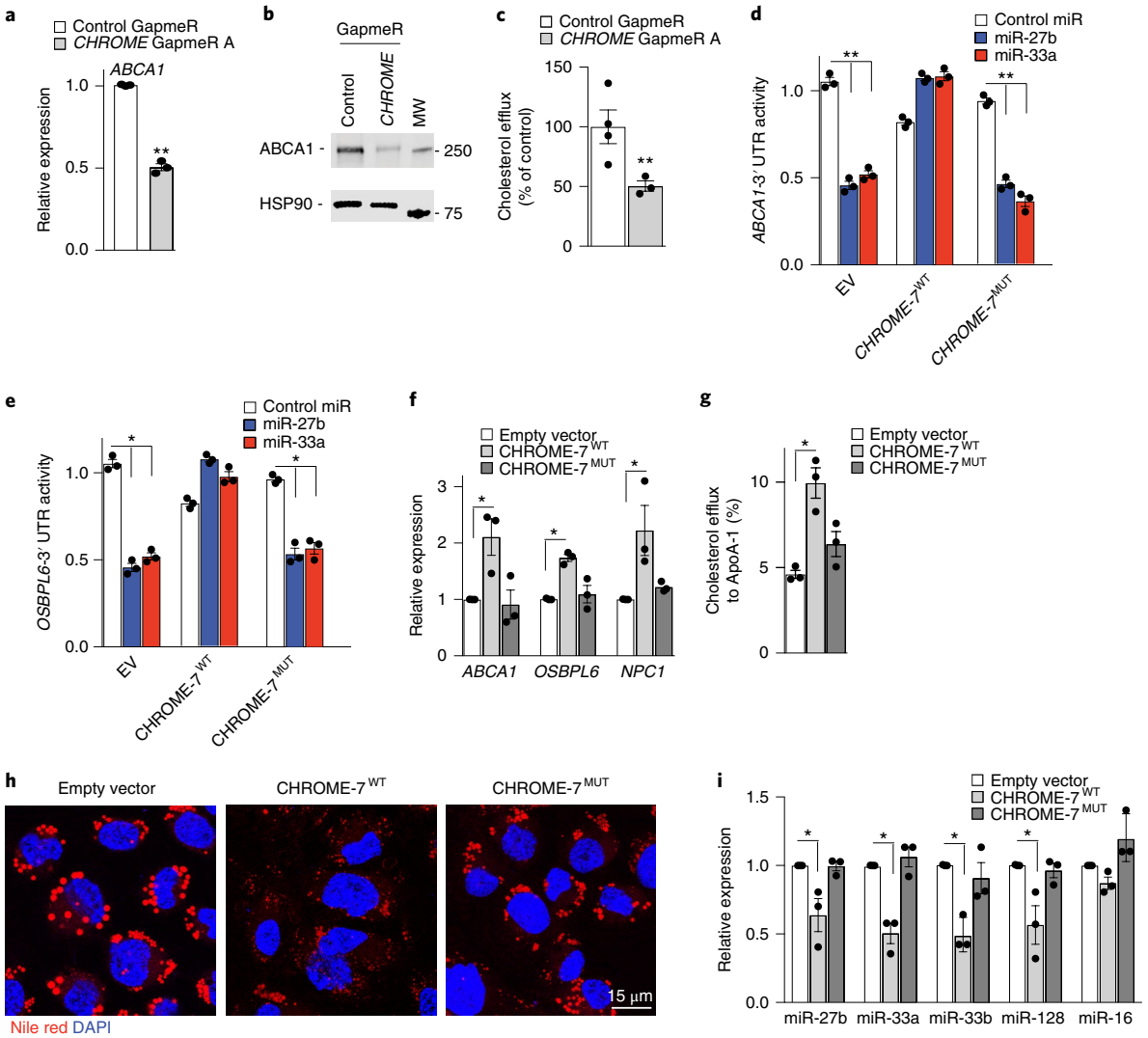

Fig. 6 | CHROME regulates cholesterol efflux in macrophages through its interaction with miRNAs. a, qPCR analysis of *ABCA1* mRNA in THP-1 macrophages transfected with control or CHROME-targeting GapmeRs. Data are the mean ± s.e.m. of three independent experiments. **b**, Western blot of ABCA1 and HSP90 (internal control) protein in THP-1 macrophages transfected with control or CHROME-targeting GapmeRs. A molecular weight (MW) marker is shown on the right. Data are representative of three independent experiments. **c**, Measurement of cholesterol efflux to exogenous APOA1 in THP-1 macrophages transfected control or CHROME-targeting GapmeRs. Data are the mean ± s.e.m. of four independent experiments. **d**,**e**, Activity of *ABCA1*-3′ UTR (**d**) and *OSBPL6*-3′ UTR (**e**) luciferase reporter genes in HEK293T cells expressing empty vector (EV), CHROME-7^{WT} or CHROME-7^{MUT} after treatment with control miR, miR-27b or miR-33 mimics. Data are the mean ± s.e.m. of three biological replicates from a single experiment. Data are representative of three independent experiments. **f**, qPCR analysis of miR-27b, miR-33 and miR-128 target genes regulating cholesterol efflux in THP-1 macrophages stably expressing empty vector, CHROME-7^{WT} or CHROME-7^{MUT}. Data are the mean ± s.e.m. of three experiments. **g**, Measurement of cholesterol efflux to APOA1 in THP-1 macrophages stably expressing empty vector, CHROME-7^{WT} or CHROME-7^{MUT}. Data are the mean ± s.e.m. of three experiments. **h**, Representative images of Nile-red-stained lipid droplet accumulation in acetylated LDL-treated THP-1 macrophages stably expressing empty vector, CHROME-7^{WT} or CHROME-7^{MUT}. Cells were stained with DAPI (blue) to visualize nuclear DNA. **i**, qPCR analysis of miRNA levels in THP-1 cells stably expressing empty vector, CHROME-7^{WT} or CHROME-7^{MUT}. miR-16 is included as a negative control. Data are the mean ± s.e.m. of three experiments. *P* values were calculated by using a two-tailed Student's *t*-test. $^{*}P \leq 0.05$, $^{**}P \leq 0.01$, $^{***}P \leq 0.001$.

CHROME regulates macrophage cholesterol efflux through non-coding RNA cross-talk. In addition to regulating hepatic HDL production, the efflux of excess cellular cholesterol is essential to maintain homeostasis in peripheral tissues, particularly the artery wall, where macrophage cholesterol efflux protects against atherosclerotic plaque formation[2]. Given that CHROME was increased in cholesterol-loaded macrophages in vitro and in atherosclerotic plaques, we next tested the effects of CHROME loss of function in THP-1 macrophages. As we observed in hepatic cells, *CHROME* GapmeR–treated THP-1 macrophages showed lower *ABCA1* mRNA and ABCA1 protein levels than control GapmeR–treated THP-1 macrophages (Fig. 6a,b and Supplementary Fig. 10a), and this was associated with lower levels of cholesterol efflux to APOA1 (Fig. 6c). Furthermore, GapmeR depletion of CHROME in THP-1 macrophages increased levels of miR-27b, miR-33a, miR-33b and miR-128, while decreasing the levels of their target mRNAs (Supplementary Fig. 10b–d), as compared with control GapmeR treatment, suggesting that CHROME acts through a similar mechanism in macrophages and hepatocytes to control cholesterol efflux. To directly test whether interactions between CHROME and miRNAs mediate its effects

on *ABCA1* expression, we assessed the ability of CHROME-7^{WT} and CHROME-7^{MUT}, in which the miRNA-binding sites are mutated, to relieve miRNA-mediated repression of *ABCA1*. To do so, we transfected HEK293T cells with a human *ABCA1*-3′ UTR luciferase reporter construct and empty vector, CHROME-7^{WT} or CHROME-7^{MUT}, and then subsequently treated them with miR-27b, miR-33a or control mimics. In cells expressing control empty vector, overexpression of miR-27b or miR-33a reduced *ABCA1*-3′ UTR luciferase activity compared with that of the control mimic, as expected (Fig. 6d). In contrast, miR-27b and miR-33a did not repress *ABCA1*-3′ UTR luciferase activity in CHROME-7^{WT}-expressing cells (Fig. 6d). This protection required the miRNA response elements in CHROME, as miR-27b and miR-33a reduced *ABCA1*-3′ UTR luciferase activity in CHROME-7^{MUT}-expressing cells to levels comparable to those observed in empty-vector-transfected cells (Fig. 6d). Moreover, similar results were obtained using a 3′ UTR-luciferase reporter construct for *OSBPL6* (Fig. 6e), which is another shared target of miR-27b and miR-33a/b that regulates cholesterol efflux. We then generated THP-1 cell lines that expressed comparable levels of CHROME-7^{WT}, CHROME-7^{MUT} or empty vector by retroviral transduction (Supplementary Fig. 10e). In agreement with the ability of CHROME to protect the *ABCA1* and *OSBPL6* 3′ UTRs from miRNA-mediated repression, CHROME-7^{WT}-expressing THP-1 macrophages showed higher levels of *ABCA1*, *OSBPL6* and *NPC1* mRNA (Fig. 6f), greater cholesterol efflux to APOA1 (Fig. 6g) and reduced accumulation of cytoplasmic lipid droplets (Fig. 6h) than did empty vector-expressing THP-1 macrophages. These differences were associated with lower levels of miR-27b, miR-33a, miR-33b and miR-128 in CHROME-7^{WT}-expressing THP-1 macrophages than in empty vector-expressing macrophages (Fig. 6i), a result consistent with the ability of CHROME to functionally deplete these miRNAs. Notably, no differences in miR-27b, miR-33a, miR-33b or miR-128 levels, *ABCA1*, *OSBPL6* and *NPC1* expression or cholesterol efflux and lipid droplet burden were observed between CHROME-7^{MUT}- and empty vector- expressing THP-1 macrophages (Fig. 6f–i). Collectively, these data suggest that the ability of CHROME to regulate cellular cholesterol efflux and lipid droplet burden depends on interactions at its miRNA response elements.

Discussion

Our work identifies a primate-specific lncRNA, CHROME, which is increased in the setting of human atherosclerotic vascular disease and contributes to the regulation of cholesterol homeostasis. We find that CHROME levels are elevated in the plasma and arterial plaques of individuals with cardiovascular disease compared with healthy controls, and its expression is regulated in response to dietary and cellular cholesterol challenge. Mechanistic studies reveal a role for CHROME in the response of hepatocytes and macrophages to cholesterol overload, through the upregulation of cholesterol efflux and HDL biogenesis. The expression of CHROME is upregulated in vitro and in vivo by activation of the sterol-activated transcription factor LXR, which controls the expression of a number of genes involved in the response to cholesterol excess. Using gain- and loss-of-function studies, we establish that CHROME curbs the actions of the functionally related miRNAs miR-27b, miR-33a, miR-33b and miR-128 to derepress their collective target genes, most notably those involved in cholesterol efflux and reverse cholesterol transport. This LXR-regulated mechanism enhances the ability of the cell to respond to the changing environment by removing existing post-transcriptional ‘brakes’ on cholesterol efflux, coincident with LXR-induced transcription of genes involved in the response to cholesterol excess. Together, our findings uncover an intricate interplay among noncoding RNA species for the fine tuning of cholesterol metabolism gene networks, and expand understanding of the regulatory mechanisms that govern human cholesterol homeostasis in health and disease.

Many human lncRNAs exhibit low evolutionary conservation[40], as is the case for CHROME. Phylogenetic analyses suggest that *CHROME* emerged in the primate lineage (Supplementary Fig. 1b), and we did not detect shared synteny in other species (Supplementary Fig. 1c). Our studies in nonhuman primates show that the expression of CHROME is upregulated in the liver when animals are fed a cholesterol-enriched diet or after short-term treatment with an LXR agonist. Using primary human hepatocytes, we identify an important role for CHROME in the efflux of cholesterol and phospholipid to APOA1, processes that are critical to the production of nascent HDL particles. In a related process, we show that CHROME also regulates efflux of excess cholesterol from macrophages, which mediate the clearance of cholesterol-rich lipoproteins that can accumulate in tissues, such as the arterial wall. The primate specificity of CHROME precludes in vivo studies of its effects on HDL metabolism and cholesterol efflux in typical preclinical animal models, such as mice. Nevertheless, loss-of-function studies in primary human hepatocytes reveal a role for CHROME in regulating HDL biogenesis, thus supporting our observational data in a patient cohort in which a positive correlation between CHROME and plasma levels of HDL-C is shown. Further testing of the ability of CHROME to regulate reverse cholesterol transport in vivo will require loss-of-function studies in nonhuman primates.

Cholesterol levels in the cell, tissue and organism are dynamically controlled by a complex network of feedback mechanisms that maintain cholesterol homeostasis. In the past decade, studies have revealed the critical contributions of miRNAs in the post-transcriptional regulation of genes that control cholesterol homeostasis[6], particularly the cholesterol efflux pathway[41]. The *ABCA1* mRNA interacts with multiple miRNAs, including miR-20 (ref. [42]), miR-27b[11,14], miR-33a and miR-33b[7,8], miR-128 (ref. [15]), miR-144 (refs [12,13]) and miR-148 (ref. [15]), which collectively impart post-transcriptional repression of the ABCA1 transporter. Inhibition of those individual miRNAs in vitro by using antisense oligonucleotides can increase ABCA1 protein and cholesterol efflux up to twofold (refs [7,8,11–15,42]), and delivery of miR-33a/b[7,8,43–45], miR-128 (ref. [15]) or miR-144 (refs [12,13]) inhibitors to mice or monkeys can raise plasma levels of HDL cholesterol by up to 50%. Therefore the ability of CHROME to simultaneously inhibit miR-27b, miR-33a, miR-33b and miR-128 provides a coordinated mechanism to relieve this potent post-transcriptional repression of the cholesterol efflux pathway. Furthermore, each variant of CHROME contains multiple binding sites for its interacting-miRNAs, which each repress multiple common target genes in lipid metabolism pathways, thus providing a mechanism for substantial regulatory cross-talk by CHROME. As levels of distinct miRNAs may vary by cell type and condition, the ability of CHROME to restrain the actions of a set of miRNAs with shared biological functions allows for greater flexibility in the dynamic adjustment of cellular cholesterol efflux in discrete cell types, such as macrophages, enterocytes and hepatocytes, which each express *ABCA1* and have distinct roles in reverse cholesterol transport and protection from atherosclerosis[46,47].

We show that the interactions of CHROME with miR-27b, miR-33a, miR-33b and miR-128 are necessary for its function in maintaining cholesterol homeostasis, as its ability to regulate the expression of *ABCA1*, cholesterol efflux and lipid droplet burden depend directly on the integrity of its binding sites for those miRNAs. Although the exact mechanisms by which CHROME titrates the availability of its miRNA binding partners remains unclear, our finding of CHROME in P-bodies opens the possibility that it traffics bound miRNAs to this granule for destabilization or degradation. Complexes between miRNA and the RNA-induced silencing complex can have half-lives of days or more[48]; thus, CHROME-mediated compartmentalization of miRNAs in P-bodies could accelerate their turnover or alternatively compromise their function through sequestration. Further studies will be needed to understand

the spatiotemporal dynamics of the associations between CHROME and miRNAs, as well as other factors that may influence these interactions. For example, interactions of cytoplasmic lncRNAs and miRNAs are likely to be influenced by subcellular microenvironments that may increase local concentrations of RNAs and RNA-binding proteins, as has been observed in neurons[49]. Furthermore, lncRNAs may interact with RNA-binding proteins that may modify lncRNA stability, localization and the chemical (for example, methylation) or secondary structure[50]. The identification of CHROME, and other lncRNAs of similar function, provides a possibility to begin to investigate the mechanisms that underlie such interactions.

Our findings also reveal the expanding roles for noncoding RNAs in mediating cross-talk between the LXR and SREBP2 transcription factors, which regulate opposing gene programmes in the cholesterol overloaded and cholesterol-depleted states. Recent studies have established that activation of LXR inhibits the expression of genes involved in cholesterol biosynthesis, including *SREBF2*, by upregulating the lncRNA LeXis, which sequesters the transcriptional cofactor RALY away from the promoters of cholesterol biosynthetic genes[23]. Conversely, we and others have shown that SREBP2 represses the expression of genes involved in cholesterol efflux and reverse cholesterol transport by upregulating expression of miR-33a[7,8], which potently represses *ABCA1* and other genes contributing to cholesterol efflux and excretion (for example, *OSBPL6* (ref. [9]), *NPC1* (refs [7,8]), *ATG5* (ref. [51]), *ABCB11* (ref. [10]) and *ATP8B1* (ref. [10])). The identification of CHROME as an LXR-regulated lncRNA that represses the actions of miR-33a, expands this paradigm of reciprocal cross-talk between LXR and SREBP2 mediated by noncoding RNAs. In addition, our RNA-seq analyses suggest a role for CHROME in the regulation of fatty-acid oxidation and the acute-phase response in hepatocytes. As miR-33, miR-27b and miR-128 have been shown to repress genes regulating β-oxidation of fatty acids (for example, *CROT* and *CPT1A*), the interaction of CHROME with these miRNAs is likely to underlie its effects on fatty-acid oxidation. The mechanisms by which CHROME alters the acute phase response are less clear, and further studies will be needed to investigate the role of CHROME in the inflammatory response in hepatocytes and macrophages. Collectively, our data identify CHROME as a component of the multilayered regulatory circuitry that is activated in response to cellular and systemic cholesterol overload, and unveil the regulatory cross-talk between noncoding RNAs that sustains cholesterol homeostasis in humans.

Methods

Human studies. All human studies complied with relevant ethical regulations. To assess the levels of CHROME RNA in individuals with coronary artery disease, we identified patients with established vascular disease in ongoing studies (NCT02106429 and NCT01897103)[52]. Plasma samples (from patients with coronary artery disease ($n=14$) or healthy control subjects ($n=33$)) were collected in accordance with the policies of New York University Langone Medical Center (NYULMC). All studies were approved by the NYULMC ethics committee. RNA was isolated from the plasma as described below. To measure CHROME expression in human healthy arterial plaques and atherosclerotic plaques, we obtained tissues and clinical data from patients undergoing surgery for stable or unstable carotid stenosis at the Department of Vascular Surgery, Karolinska University Hospital, Stockholm, Sweden, in collaboration with the Biobank of Karolinska Endarterectomies (BiKE) at the Centre for Molecular Medicine, Karolinska Institute. Gene-expression analyses were performed in material obtained from individuals prospectively enrolled in the BiKE study between 2005 and 2008; a total of $n=127$ plaques from patients and $n=10$ normal arteries (undiseased macroscopically atherosclerosis-free arteries, iliac and one aorta) were obtained from organ donors without any current or history of cardiovascular disease. No power calculation or selection of patients on the basis of any other clinical criteria other than symptomatic or asymptomatic carotid disease was done for this purpose; instead tissues were arrayed according to sample availability and RNA quality. All samples were collected with informed consent from patients, organ donors or their guardians. The BiKE study is approved by the Ethical Committee of Northern Stockholm with the following ethical permits: EPN DNr 95-276/277; DNr 02-146; DNr 02-147, DNr 2005/83-31; DNR 2009/512-31/2; 2012/619-32. The project is performed under the Swedish biobank regulations and prospective sampling is approved through an informed consent procedure (DNr 2009/512-31/2). BiKE is registered at Socialstyrelsen (The National Board of Health and Welfare) and the Biobank of Karolinska and approved by the Swedish Data Inspection Agency (approval date/number 2002-09-30 DNr 916-2002). The BiKE study cohort demographics, details of sample collection, processing and analyses have been previously described[53]. Gene-expression profiles were analyzed with Affymetrix HG-U133 plus 2.0 Genechip microarrays. Robust multiarray average normalization and correction for batch effects was performed, and processed gene-expression data were transformed to a $\log_2$ scale. The microarray dataset is available from Gene Expression Omnibus (GSE21545). In situ hybridization of CHROME was performed on formalin-fixed samples of human carotid endarterectomy samples or iliac arteries as control tissues with locked nucleic acid (LNA) Detection Probes for In situ Hybridization (Exiqon) recognizing a sequence common to all CHROME variants (Supplementary Table 3) or control scramble-ISH custom LNA Detection Probe (Exiqon) at a final concentration 25 nM and labeled with digoxigenin (DIG). To measure hepatic expression of CHROME and its miRNA targets, we obtained healthy liver tissue and serum samples from individuals undergoing liver surgery, and experimental procedures were performed within the framework of the non-profit foundation HTCR Stiftung, including the patient's informed consent[54]. No power calculation or selection of patients on the basis of any other clinical criteria other than undergoing liver surgery was done for this purpose; instead tissues were arrayed according to sample availability and RNA quality. This study was approved by the Ethics Committee of the Bavarian Medical Association (Bayerische Landesärztekammer) and the Ethics Committee of the Ludwig-Maximilians-University Munich. RNA ($n=200$) was isolated and reverse transcribed (2 µg for mRNA; 1 µg for miRNA), and analyzed by qPCR as described below. Serum levels of APOA1 and HDL cholesterol were determined with an immunoturbidimetric assay (Beckman Coulter) and an enzymatic assay (Beckman Coulter), respectively, and run on an AU5800 automated analyzer (Beckman Coulter).

Animal studies. Monkeys were housed in an Association for Assessment and Accreditation of Laboratory Animal Care (AAALAC)-accredited facility under the direct care of the Wake Forest University Health Sciences (WFUHS) Animal Resources Program. All experiments were approved by the WFUHS Institutional Animal Care and Use Committee (IACUC) and complied with relevant ethical regulations. Monkeys were singly housed in climate-controlled conditions with a 12-h light and dark cycle. Male African green (*Chlorocebus aethiops*) monkeys ($n=5$ per group; age 4–9 years) maintained on a chow diet (0.002 mg per kcal cholesterol) were fed a high-fat, moderate-cholesterol (0.15 mg per kcal) diet for 8 weeks, and liver biopsies were obtained before and after diet feeding. For treatment with LXR agonist, adult male cynomolgus (*Macaca fascicularis*) monkeys (mean age 2.7 years) were fasted, anesthetized and gavaged with either vehicle or 10 mg kg^{-1} GW3965 ($n=5$ per group) daily for 2 d. Exactly 6 h after dosing on day 2, fasted monkeys were euthanized, and tissues were collected.

Cell culture. HEK293T, HepG2 and THP-1 cell lines were obtained from American Type Tissue Collection, authenticated with standard American Type Tissue Collection methods (morphology check under a microscope and growth curve analysis) and tested monthly for mycoplasma contamination. HEK293T were maintained in high-glucose DMEM (Corning) supplemented with 10% fetal bovine serum (FBS, Life Technologies) and 1% penicillin–streptomycin (Life Technologies). HepG2 cells were maintained in EMEM (Corning) with 10% non-heat-inactivated FBS and 1% penicillin–streptomycin. THP-1 cells were maintained in RPMI 1640 (Corning) with 10% FBS and 1% penicillin–streptomycin, and were differentiated into macrophages in the presence of 100 nM phorbol-12-myristate acetate (PMA, Sigma) for 48–72 h. Primary human hepatocytes were obtained from Yecuris, seeded on Coating Matrix (Life Technologies, R011K) and maintained in hepatocyte basal medium supplemented with a hepatocyte basal medium bullet kit (Lonza). To assess the response to cholesterol loading and LXR activation, we stimulated cells with 37.5 µg ml^{-1} acetylated LDL (Biomedical Technologies) for 24 h, 10 µM T0901317 (Cayman Chemical Company) for 8 or 24 h, or 10 µg ml^{-1} cholesterol–cyclodextrin (Sigma) for 72 h. For transient knockdown of LXR in THP-1 cells, SMARTpool ON-Targetplus siRNA against *LXRA* (also known as *NR1H3*) and *LXRB* (also known as *NR1H2*) (Dharmacon, 25 nM each) was used for transfection. Non-targeting siRNA was used as a control. For *LXRA* and *LXRB* knockdown studies, 48 h after transfection, cells were treated with 50 µg mL^{-1} acetylated LDL for 24 h.

RNA isolation and qPCR. Total RNA was isolated with TRIzol reagent (Invitrogen) and Direct-zol RNA MiniPrep columns (Zymo Research). RNA was reverse transcribed with an iScript cDNA Synthesis Kit (Bio-Rad Laboratories), and qPCR analysis was conducted with KAPA SYBR green Supermix (KAPA Biosystems) according to the manufacturer's instructions and quantified on a Mastercycler Realplex (Eppendorf). miRNA quantification was performed in quadruplicate with an miScript SYBR Green PCR Kit (Qiagen) with the Qiagen miScript Primer Assays listed in Supplementary Table 3. The fold change in mRNA and miRNA expression was calculated with the comparative cycle method ($2^{-\Delta\Delta C_t}$) and normalized to the housekeeping genes (*GAPDH* for mRNA; RNU-6 (*U6*) or

miR-16 for miRNA), or per microgram of RNA (for tissue profiling). For plasma samples, RNA was isolated with TRIzol reagent (4:1 v/v) followed by an RNA Clean & Concentrator-5 Plasma/Serum kit (Zymo Research). Subsequently, 5 µl of total RNA was reverse transcribed and used for qPCR. Copy numbers were determined by using standard curves of CHROME variants.

Chromatin immunoprecipitation assay. THP-1 cells differentiated with PMA were treated with 10 µM T0901317 for 8 h, and cells were treated with 1% formaldehyde to cross-link. The reaction was stopped with 0.125 M glycine, followed by washing in ice-cold PBS, and the cells were pelleted. Nuclear lysates were collected and passed through a 25-gauge needle and sonicated until chromatin was sheared to fragments of 500 to 2,000 bp,. For immunoprecipitation of LXR, 30 µg of chromatin was incubated with a cocktail of 3 µg anti-LXRα and 3 µg anti-LXRβ antibodies (Abcam, ab41902 and ab56237) or isotype-matched IgG (Abcam, ab171870). Bound chromatin was immunoprecipitated with Dynabeads Protein G (Life Technologies), and bead–chromatin complexes were washed and dissociated at 65 °C. DNA was purified with a PrepEase DNA Clean-Up Kit (Affymetrix), and 1 µl of DNA was used for qPCR.

RNA FISH. RNA FISH and simultaneous RNA and DNA detection were performed as described[55,56]. In brief, cells were fixed in 4% paraformaldehyde, permeabilized in cytoskeletal buffer, 5% Triton X-100 and vanadyl ribonucleoside complex, and subsequently stored in PBS or 70% ethanol. DNA probes (1 µg per reaction) were nick-translated with biotin-11-dUTP or digoxigenin-16-dUTP (Roche Diagnostics). RNA-specific hybridization was carried out under non-denaturing conditions in which the DNA was not accessible. For colocalization with AGO2, HEK293T cells were transfected with an AGO2–GFP plasmid (Addgene, 21981) for 24 h, and FISH was performed for CHROME as described above, or cells were fixed in 4% paraformaldehyde and blocked and permeabilized in 2.5% BSA and 0.1% Triton X-100, and stained for EDC4 with a rabbit anti-human antibody (Cell Signaling Technology, 2548) followed by fluorescent goat anti-rabbit secondary antibodies (Life Technologies, A-11011).

Gain- and loss-of-function studies. For RNA-interference studies, shRNAs targeting a region common to all CHROME variants or a non-targeting control shRNA (Supplementary Table 3) were cloned into the pLKO vector (Addgene, 8453) and transfected into HEK293T cells with packaging vectors psPAX2 (Addgene, 12260) and pMD2.G (Addgene, 12259). After 48 h, the culture medium was isolated and used to transduce HepG2 cells. Cells stably expressing the shRNAs were selected by using 5 µg ml^{-1} puromycin (Thermo Fisher Scientific). For transient knockdown of CHROME, primary human hepatocytes, HepG2 cells or PMA-differentiated THP-1 cells were transfected with 62.5 nM LNA GapmeRs targeting a common regions of all CHROME variants or negative control A (Exiqon), by using Lipofectamine RNAiMax (Life Technologies). To create CHROME-overexpressing cell lines, *CHROME* cDNAs were obtained from Genscript, cloned into the pMSCV-PIG vector (Addgene, 21654) and transfected into HEK293T cells with packaging vectors pCMV-VSV-G (Addgene, 8454) and pCMV-Gag-Pol (Cell Biolabs, RV-111). After 48 h, the culture medium was isolated and used to transduce THP-1 or HepG2 cells, and cells were selected with puromycin (5 µg ml^{-1}, Thermo Fisher Scientific). To mutate the predicted binding sites for miR-27b, miR-33a, miR-33b and miR-128 within CHROME-7, we deleted the seed match sequence for those miRNAs with a QuikChange XL kit (Stratagene), by using the primers indicated in Supplementary Table 3. CHROME-7^{MUT}-expressing cell lines were generated as described above. All constructs were confirmed by sequencing.

RNA-seq. RNA was isolated in triplicate from HepG2 cells that expressed shRNAs against all CHROME variants or control shRNA. RNA was used to generate barcoded cDNA libraries by using a TruSeq RNA Sample Preparation kit (Illumina). Indexed libraries were pooled and sequenced (paired-end 50- or 100-bp reads) on the Illumina HiSEQ platform. RNA-seq reads were aligned by using the STAR Aligner against hg19 annotations. Gene counting was done with featureCounts. Raw counts were normalized, and differential-expression analysis was performed by using DESeq2. RNA-seq data have been deposited in the Gene Expression Omnibus under accession number GSE97469.

Bioinformatics. The coding potential of CHROME variants was predicted by using the Coding Potential Calculator (http://cpc.cbi.pku.edu.cn/programs/cpc.do) and the Coding Potential Tool Assessment (http://lilab.research.bcm.edu/cpat/calculator_sub.php) algorithms. Kozak strength was determined by using the NCBI ORFFinder (http://atgpr.dbcls.jp/). LXR response elements (LXREs) in the regulatory regions of CHROME were defined by using JASPAR (http://jaspar.genereg.net/). The mean free energy changes associated with the formation of CHROME–miRNA complexes were calculated by using RNAcofold (http://rna.tbi.univie.ac.at/cgi-bin/RNAWebSuite/RNAcofold.cgi), which predicts secondary structures of single-stranded RNA sequences on dimer formation. This algorithm takes the length of the transcript and secondary structure into account. One thousand randomly selected sections of the human genome with a length of 21–22 nucleotides were run through RNAcofold, along with annotated miRNA sequences including miR-27b, miR-128, miR-33a, miR-33b and miR-16, and aligned pairwise with CHROME transcripts. For RNA-seq analyses, ingenuity pathway analysis (Qiagen) was used to evaluate the most significantly altered genes and pathways. Cumulative distribution function analysis was performed by using the statistical software package R v.2.8.0 (www.r-project.org)[57] for predicted targets of miR-27b, miR-33a/b, miR-128 and miR-122 versus non-targets (defined by using Targetscan; http://www.targetscan.org/vert_72/). Statistical enrichment of predicted miR-33a/b, miR-27b and miR-128 target sites among differentially regulated genes in HepG2 RNA-seq datasets was performed by using miRhub as described[58].

Western blots. Protein was extracted in RIPA buffer (Cell Signaling) with protease and phosphatase inhibitors (Roche) and subsequently normalized with a Pierce BCA Protein Assay Kit (Thermo Fisher Scientific). Samples (30 µg per well) were electrophoresed on 4–20% TGX-gradient gels (Bio-Rad Laboratories) and transferred to nitrocellulose membranes at 125 V for 2 h. Membranes were incubated overnight with the specified antibodies directed against ABCA1 (Novus Biologicals, NB400-105) and HSP90 (BD Biosciences, 610419). Proteins were visualized by using appropriate secondary antibodies and scanned with an Odyssey Imaging System (Li-Cor Biosciences). Quantification was performed in Image Studio software (Li-Cor Biosciences).

Cholesterol efflux assay and neutral lipid staining. For cholesterol efflux assays, HepG2 or THP-1 cells stably expressing CHROME variants were seeded in 24-well plates at a density of 1×10^6 cells, and THP-1 cells were treated with PMA as described above. Primary hepatocytes were seeded at 2×10^5 in 48-well plates and transfected with control or CHROME-targeting GapmeRs. Cells were labeled with 0.5 µCi ml^{-1} of ^{3}H-cholesterol (PerkinElmer) for 24 h, washed twice with PBS and then incubated with 2 mg ml^{-1} fatty-acid-free BSA (Sigma-Aldrich) in medium for 24 h. To induce efflux, we added 50 µg ml^{-1} human APOA1 in fatty-acid-free medium, and supernatants were collected after 8 or 24 h. APOA1-dependent efflux was expressed as a percentage of total cell ^{3}H-cholesterol content. To visualize neutral lipids, we treated THP-1 cells stably expressing CHROME variants with PMA as described above and then incubated them with 37.5 µg ml^{-1} acetylated LDL for 24 h. Cells were then stained by using Nile red (Thermo Fisher Scientific) as previously described[59].

Endogenous APOA1 lipidation. To assess phospholipid efflux to endogenous APOA1 in primary human hepatocytes, we seeded cells at 2×10^5 in 48-well plates and transfected them with GapmeRs, as described above. Hepatocytes were labeled with 5 µCi ml^{-1} of ^{14}C-choline chloride (PerkinElmer) for 48 h, washed twice and incubated for 24 h in serum-free HCM supplemented with 10 µM T0901317 (Cayman Chemical Company). APOA1 secreted into the cell culture supernatant was immunoprecipitated from the culture medium with polyclonal anti-human APOA1 antibody (EMD Millipore, 178422) and protein G–sepharose (Sigma-Aldrich), then washed in PBS, and scintillation counting was performed to assess the amount of phospholipid efflux.

Immunoprecipitation of AGO2. AGO2 was immunoprecipitated from primary human hepatocytes or PMA-differentiated THP-1 macrophages by using a MagnaRIP RNA-Binding Protein Immunoprecipitation Kit (EMD Millipore) according to the manufacturers' instructions. In brief, an antibody targeting human AGO2 (Millipore, RIPAb+ AGO2, 03-110) or an isotype-matched control antibody (EMD Millipore, CS200621) was bound to magnetic beads and incubated with lysed cells at 4 °C for 24 h. Beads were isolated, and coprecipitated RNA was purified, cleaved from AGO2 by proteinase K and purified by using TRIzol reagent. PCR analysis of total RNA was performed to detect CHROME, and enrichment of CHROME variants in the AGO2 fraction was determined by correcting for both *GAPDH* levels and the fraction that coprecipitated with IgG antibodies.

MS2-TRAP. MS2-TRAP was performed as previously described[37]. In brief, HEK293T cells were transfected with plasmids for expresison of CHROME-1, CHROME-3 or CHROME-7 in frame with an MS2-binding sequence, together with a YFP-tagged MS2-binding protein expression plasmid for 24 h. MS2-binding protein was immunoprecipitated by using an antibody against GFP (Roche Diagnostics, 118144600001) or isotype-matched IgG control antibody (EMD Millipore, CS200621), and coprecipitated RNA was isolated by using TRIzol. Total RNA was analyzed by qPCR for miR-16, miR-27b, miR-33a/b, miR-128, miR-155, miR-224 and *U6*. Enrichment of miRNAs bound to CHROME was determined by correction for *U6* levels, the fraction that coprecipitated with IgG antibodies and the expression levels of miRNAs in cells expressing the empty control plasmid.

Cholesterol biosynthesis and LDL uptake. HepG2 cells were seeded and incubated with 5 µCi ml^{-1} of ^{3}H-acetate (Amersham) in EMEM supplemented with 10% lipoprotein-deficient serum. After 24 h, cells were lysed with 0.25 N NaOH, and lipid extraction was performed as previously described[60]. The organic layer was dried under N_2 gas, and samples were resuspended in hexane. Lipids were separated by thin-layer chromatography in the solvent system hexane:diethyl ether:acetic acid (105:45:1). The bands corresponding to cholesterol fractions were collected, and radioactivity was determined by liquid scintillation counting. Data

were normalized to cellular protein levels obtained with a Pierce BCA Protein Assay Kit. To measure LDL uptake, we seeded HepG2 cells in poly-D-lysine-coated Labtek slides and incubated them for 4 h with Dil–LDL (10 μg ml^{-1}, AlfaAesar) in EMEM supplemented with 2 mg ml^{-1} BSA. Intracellular LDL was detected by microscopy (Leica SP5), and the fluorescence intensity was quantified by using Fiji software (https://fiji.sc/) from six fields of view.

miRNA degradation. HEK293T cells were stransfected with a wild-type or mutant CHROME-7 expression plasmid and miRNA mimics at various concentrations (25 nM, 50 nM and 100 nM) with Lipofectamine 2000 (Invitrogen) overnight. miRNA expression was quantified by qPCR. Control non-targeting mimic and an empty vector plasmid were used for normalization.

3′ UTR luciferase experiments. Human *ABCA1*- and human *OSBPL6*-3′ UTR luciferase/*Renilla* reporter constructs were obtained from GeneCopoeia. HEK293T cells were transfected with 1 μg of the 3′ UTR luciferase reporter vector and wild-type or mutant CHROME expression plasmid. Cells were then treated with 50 nM miRNA mimic or control mimic by using Lipofectamine 2000 (Invitrogen) in a 96-well plate. Subsequently, 3′ UTR activity was assessed by measuring luciferase activity with the Dual Glo Luciferase Assay System (Promega). Firefly luciferase activity was normalized to *Renilla* luciferase activity.

Statistics. The statistical significance of differences of three or more independent biological replicates was evaluated with Student's *t*-test or two-way analysis of variance (ANOVA) for multiple group comparisons. The Tukey and Dunnett tests were used as follow-up tests to the ANOVAs; the Tukey test was used to compare every mean with every other mean, and the Dunnett test was used when comparing every mean to a control mean. For human liver gene-expression studies, data were quantile-normalized with the statistical software package R v.2.8.0 (ref. [57]). The normality of distribution was tested with the Kolmogorov–Smirnov test implemented in PRISM statistical software (GraphPad). No significant effects of age and sex on gene-expression levels were detected. Spearman correlation coefficients between gene-expression data and serum APOA1 and HDL cholesterol levels and levels of significance were calculated by using SAS statistic software (SAS v.9.3, SAS Institute).

Reporting Summary. Further information on research design is available in the Nature Research Reporting Summary linked to this article.

Data availabilty

The Biobank of Karolinska Endarterectomies (BiKE) microarray dataset has been deposited in the Gene Expression Omnibus (GEO) and is available under accession GSE21545. HepG2 RNA-sequencing datasets have been deposited in GEO under accession GSE97469. Data that support the plots within this paper and other findings of this study are available from the corresponding author upon reasonable request.

Received: 15 July 2018; Accepted: 16 October 2018;
Published online: 3 December 2018

References

1. Goedeke, L. & Fernandez-Hernando, C. Regulation of cholesterol homeostasis. *Cell. Mol. Life Sci.* **69**, 915–930 (2012).
2. Siddiqi, H. K., Kiss, D. & Rader, D. HDL-cholesterol and cardiovascular disease: rethinking our approach. *Curr. Opin. Cardiol.* **30**, 536–542 (2015).
3. Lee, S. D. & Tontonoz, P. Liver X receptors at the intersection of lipid metabolism and atherogenesis. *Atherosclerosis* **242**, 29–36 (2015).
4. Scacalossi, K. R., van Solingen, C. & Moore, K. J. Long non-coding RNAs regulating macrophage functions in homeostasis and disease. *Vascul. Pharmacol.* https://doi.org/10.1016/j.vph.2018.02.011 (2018).
5. van Solingen, C., Scacalossi, K. R. & Moore, K. J. Long noncoding RNAs in lipid metabolism. *Curr. Opin. Lipidol.* **29**, 224–232 (2018).
6. Feinberg, M. W. & Moore, K. J. microRNA regulation of atherosclerosis. *Circ. Res.* **118**, 703–720 (2016).
7. Najafi-Shoushtari, S. H. et al. microRNA-33 and the SREBP host genes cooperate to control cholesterol homeostasis. *Science* **328**, 1566–1569 (2010).
8. Rayner, K. J. et al. MiR-33 contributes to the regulation of cholesterol homeostasis. *Science* **328**, 1570–1573 (2010).
9. Ouimet, M. et al. miRNA targeting of oxysterol-binding protein-like 6 regulates cholesterol trafficking and efflux. *Arterioscler. Thromb. Vasc. Biol.* **36**, 942–951 (2016).
10. Allen, R. M. et al. miR-33 controls the expression of biliary transporters, and mediates statin- and diet-induced hepatotoxicity. *EMBO Mol. Med.* **4**, 882–895 (2012).
11. Goedeke, L. et al. miR-27b inhibits LDLR and ABCA1 expression but does not influence plasma and hepatic lipid levels in mice. *Atherosclerosis* **243**, 499–509 (2015).
12. de Aguiar Vallim, T. Q. et al. microRNA-144 regulates hepatic ATP binding cassette transporter A1 and plasma high-density lipoprotein after activation of the nuclear receptor farnesoid X receptor. *Circ. Res.* **112**, 1602–1612 (2013).
13. Ramirez, C. M. et al. Control of cholesterol metabolism and plasma high-density lipoprotein levels by microRNA-144. *Circ. Res.* **112**, 1592–1601 (2013).
14. Liu, X. H. et al. lnc RNA HOTAIR functions as a competing endogenous RNA to regulate HER2 expression by sponging miR-331-3p in gastric cancer. *Mol. Cancer* **13**, 92 (2014).
15. Wagschal, A. et al. Genome-wide identification of microRNAs regulating cholesterol and triglyceride homeostasis. *Nat. Med.* **21**, 1290–1297 (2015).
16. Quinn, J. J. & Chang, H. Y. Unique features of long non-coding RNA biogenesis and function. *Nat. Rev. Genet.* **17**, 47–62 (2016).
17. Palazzo, A. F. & Lee, E. S. Non-coding RNA: what is functional and what is junk? *Front. Genet.* **6**, 2 (2015).
18. Schmitz, S. U., Grote, P. & Herrmann, B. G. Mechanisms of long noncoding RNA function in development and disease. *Cell. Mol. Life Sci.* **73**, 2491–2509 (2016).
19. Freedman, J. E. & Miano, J. M. Challenges and opportunities in linking long noncoding RNAs to cardiovascular, lung, and blood diseases. *Arterioscler. Thromb. Vasc. Biol.* **37**, 21–25 (2017).
20. Yan, C., Chen, J. & Chen, N. Long noncoding RNA MALAT1 promotes hepatic steatosis and insulin resistance by increasing nuclear SREBP-1c protein stability. *Sci. Rep.* **6**, 22640 (2016).
21. Liu, C. et al. Long noncoding RNA H19 interacts with polypyrimidine tract-binding protein 1 to reprogram hepatic lipid homeostasis. *Hepatology* **67**, 1768–1783 (2018).
22. Li, D. et al. Identification of a novel human long non-coding RNA that regulates hepatic lipid metabolism by inhibiting SREBP-1c. *Int. J. Biol. Sci.* **13**, 349–357 (2017).
23. Sallam, T. et al. Feedback modulation of cholesterol metabolism by the lipid-responsive non-coding RNA *LeXis*. *Nature* **534**, 124–128 (2016).
24. Sallam, T. et al. Transcriptional regulation of macrophage cholesterol efflux and atherogenesis by a long noncoding RNA. *Nat. Med.* **24**, 304–312 (2018).
25. Pasmant, E., Sabbagh, A., Vidaud, M. & Bieche, I. *ANRIL*, a long, noncoding RNA, is an unexpected major hotspot in GWAS. *FASEB J.* **25**, 444–448 (2011).
26. Holdt, L. M. & Teupser, D. Recent studies of the human chromosome 9p21 locus, which is associated with atherosclerosis in human populations. *Arterioscler. Thromb. Vasc. Biol.* **32**, 196–206 (2012).
27. Nsengimana, J. et al. Enhanced linkage of a locus on chromosome 2 to premature coronary artery disease in the absence of hypercholesterolemia. *Eur. J. Hum. Genet.* **15**, 313–319 (2007).
28. North, K. E., Martin, L. J., Dyer, T., Comuzzie, A. G. & Williams, J. T. HDL cholesterol in females in the Framingham Heart Study is linked to a region of chromosome 2q. *BMC Genet.* **4**, S98 (2003).
29. Kapusta, A. et al. Transposable elements are major contributors to the origin, diversification, and regulation of vertebrate long noncoding RNAs. *PLoS Genet.* **9**, e1003470 (2013).
30. Perisic, L. et al. Profiling of atherosclerotic lesions by gene and tissue microarrays reveals PCSK6 as a novel protease in unstable carotid atherosclerosis. *Arterioscler. Thromb. Vasc. Biol.* **33**, 2432–2443 (2013).
31. Moore, K. J. & Tabas, I. Macrophages in the pathogenesis of atherosclerosis. *Cell* **145**, 341–355 (2011).
32. Cabili, M. N. et al. Localization and abundance analysis of human lncRNAs at single-cell and single-molecule resolution. *Genome Biol.* **16**, 20 (2015).
33. Lennox, K. A. & Behlke, M. A. Cellular localization of long non-coding RNAs affects silencing by RNAi more than by antisense oligonucleotides. *Nucleic Acids Res.* **44**, 863–877 (2016).
34. John, S. et al. Kinetic complexity of the global response to glucocorticoid receptor action. *Endocrinology* **150**, 1766–1774 (2009).
35. Davalos, A. et al. miR-33a/b contribute to the regulation of fatty acid metabolism and insulin signaling. *Proc. Natl Acad. Sci. USA* **108**, 9232–9237 (2011).
36. Vickers, K. C. et al. microRNA-27b is a regulatory hub in lipid metabolism and is altered in dyslipidemia. *Hepatology* **57**, 533–542 (2013).
37. Yoon, J. H., Srikantan, S. & Gorospe, M. MS2-TRAP (MS2-tagged RNA affinity purification): tagging RNA to identify associated miRNAs. *Methods* **58**, 81–87 (2012).
38. Liu, J., Valencia-Sanchez, M. A., Hannon, G. J. & Parker, R. microRNA-dependent localization of targeted mRNAs to mammalian P-bodies. *Nat. Cell Biol.* **7**, 719–723 (2005).
39. Hubstenberger, A. et al. P-body purification reveals the condensation of repressed mRNA regulons. *Mol. Cell* **68**, 144–157 (2017).
40. Ulitsky, I. Evolution to the rescue: using comparative genomics to understand long non-coding RNAs. *Nat. Rev. Genet.* **17**, 601–614 (2016).
41. Rayner, K. J. & Moore, K. J. microRNA control of high-density lipoprotein metabolism and function. *Circ. Res.* **114**, 183–192 (2014).

42. Liang, B. et al. microRNA-20a/b regulates cholesterol efflux through post-transcriptional repression of ATP-binding cassette transporter A1. *Biochim. Biophys. Acta* **1862**, 929–938 (2017).
43. Marquart, T. J., Allen, R. M., Ory, D. S. & Baldan, A. miR-33 links SREBP-2 induction to repression of sterol transporters. *Proc. Natl Acad. Sci. USA* **107**, 12228–12232 (2010).
44. Rayner, K. J. et al. Inhibition of miR-33a/b in non-human primates raises plasma HDL and lowers VLDL triglycerides. *Nature* **478**, 404–407 (2011).
45. Rayner, K. J. et al. Antagonism of miR-33 in mice promotes reverse cholesterol transport and regression of atherosclerosis. *J. Clin. Invest.* **121**, 2921–2931 (2011).
46. Abumrad, N. A. & Davidson, N. O. Role of the gut in lipid homeostasis. *Physiol. Rev.* **92**, 1061–1085 (2012).
47. Westerterp, M. et al. ATP-binding cassette transporters, atherosclerosis, and inflammation. *Circ. Res.* **114**, 157–170 (2014).
48. Ameres, S. L. et al. Target RNA-directed trimming and tailing of small silencing RNAs. *Science* **328**, 1534–1539 (2010).
49. Cajigas, I. J. et al. The local transcriptome in the synaptic neuropil revealed by deep sequencing and high-resolution imaging. *Neuron* **74**, 453–466 (2012).
50. Jens, M. & Rajewsky, N. Competition between target sites of regulators shapes post-transcriptional gene regulation. *Nat. Rev. Genet.* **16**, 113–126 (2015).
51. Ouimet, M. et al. microRNA-33 regulates macrophage autophagy in atherosclerosis. *Arterioscler. Thromb. Vasc. Biol.* **37**, 1058–1067 (2017).
52. Montenont, E. et al. Platelet WDR1 suppresses platelet activity and associates with cardiovascular disease. *Blood* **128**, 2033–2042 (2016).
53. Perisic, L. et al. Gene expression signatures, pathways and networks in carotid atherosclerosis. *J. Intern. Med.* **279**, 293–308 (2016).
54. Thasler, W. E. et al. Charitable state-controlled foundation human tissue and cell research: ethic and legal aspects in the supply of surgically removed human tissue for research in the academic and commercial sector in Germany. *Cell Tissue Bank* **4**, 49–56 (2003).
55. Johnson, C. V., Singer, R. H. & Lawrence, J. B. Fluorescent detection of nuclear RNA and DNA: implications for genome organization. *Methods Cell Biol.* **35**, 73–99 (1991).
56. Tam, R., Smith, K. P. & Lawrence, J. B. The 4q subtelomere harboring the FSHD locus is specifically anchored with peripheral heterochromatin unlike most human telomeres. *J. Cell. Biol.* **167**, 269–279 (2004).
57. Ihaka, R. & Gentleman, R. A language for data analysis and graphics. *J. Comput. Graph. Stat.* **5**, 299–314 (1996).
58. Baran-Gale, J., Fannin, E. E., Kurtz, C. L. & Sethupathy, P. Beta cell 5′-shifted isomiRs are candidate regulatory hubs in type 2 diabetes. *PLoS ONE* **8**, e73240 (2013).
59. Listenberger, L. L. & Brown, D. A. Fluorescent detection of lipid droplets and associated proteins. *Curr. Protoc. Cell. Biol.* **24**, 24.2.1–24.2.11 (2007).
60. Folch, J., Lees, M. & Sloane Stanley, G. H. A simple method for the isolation and purification of total lipides from animal tissues. *J. Biol. Chem.* **226**, 497–509 (1957).

Acknowledgements

This work was supported by grants from the NIH (R01HL119047 (K.J.M.), R35HL135799 (K.J.M.), R01HL117226 (M.J.G.), T32HL098129 (E.J.H., C.v.S.), R01HL114978 (J.S.B.), R00HL088528 (R.E.T.), R01HL111932 (R.E.T.), R01HL128996 (K.C.V.), P01HL116263 (K.C.V.), R01DK105965 (P.S.)), the American Heart Association (14POST20180018 (C.v.S.), 13CRP14410042 (J.S.B.)), FINOVI (E.P.R.), the Swedish Society for Medical Research (L.P.M.) and the Heart and Lung Foundation (L.P.M.), the German Research Foundation CRC 1123 Project B1 (D.T. and L.M.H.), German Biobank Alliance BMBF 01EY1711C (German Ministry of Education and Research to D.T. and L.M.H.) and the Leducq Foundation CAD genomics (D.T. and L.M.H.). The BiKE study was supported by the Swedish Heart and Lung Foundation, the Swedish Research Council (K2009-65X-2233-01-3, K2013-65X-06816-30-4, 349-2007-8703), Uppdrag Besegra Stroke (P581/2011-123), the Strategic Cardiovascular Programs of Karolinska Institutet and Stockholm County Council, the Foundation for Strategic Research and the European Commission (CarTarDis, AtheroRemo, VIA, AtheroFlux projects). We thank E. A. Fisher (New York University) for helpful discussions, and S. Zhao and Q. Sheng (Vanderbilt University) for their efforts in sequencing-data analysis.

Author contributions

E.J.H., C.v.S. and K.J.M. designed the study, guided the interpretation of the results and prepared the manuscript, with input from all authors. E.J.H. and C.v.S. performed experiments and data analyses. K.R.S., M.O., M.S.A., J.P., G.J.K., M.S., B.R., K.C.V., M.K. and P.S. contributed to experiments and data analyses. S.C. created and analyzed stable cell lines. A.B. and M.O. performed in situ hybridization of human plaques. E.C., L.P.M., U.H. and L.M. processed and analyzed BiKE datasets. B.E.C. performed RNAcofold and RNAhybrid analyses. E.P.R. performed polysome fractionation experiments. R.E.T. supervised nonhuman primate studies. M.A.H. and M.J.G. performed chromatin immunoprecipitation experiments. J.S.B. provided human plasma samples and assisted in data interpretation. D.T. and L.M.H. performed human liver RNA and lipoprotein analyses.

Competing interests

K.J.M. and New York University hold a patent (US 9241950, status: issued 26 January 2016) on the use of miR-33 inhibitors to treat inflammation. All other authors have no competing interests.

Additional information

Supplementary information is available for this paper at https://doi.org/10.1038/s42255-018-0004-9.

Reprints and permissions information is available at www.nature.com/reprints.

Correspondence and requests for materials should be addressed to K.J.M.

Publisher's note: Springer Nature remains neutral with regard to jurisdictional claims in published maps and institutional affiliations.

nature research

Corresponding author(s): Kathryn J Moore

Reporting Summary

Nature Research wishes to improve the reproducibility of the work that we publish. This form provides structure for consistency and transparency in reporting. For further information on Nature Research policies, see Authors & Referees and the Editorial Policy Checklist.

Statistical parameters

When statistical analyses are reported, confirm that the following items are present in the relevant location (e.g. figure legend, table legend, main text, or Methods section).

n/a	Confirmed	
☐	☒	The exact sample size (*n*) for each experimental group/condition, given as a discrete number and unit of measurement
☐	☒	An indication of whether measurements were taken from distinct samples or whether the same sample was measured repeatedly
☐	☒	The statistical test(s) used AND whether they are one- or two-sided *Only common tests should be described solely by name; describe more complex techniques in the Methods section.*
☐	☒	A description of all covariates tested
☐	☒	A description of any assumptions or corrections, such as tests of normality and adjustment for multiple comparisons
☐	☒	A full description of the statistics including central tendency (e.g. means) or other basic estimates (e.g. regression coefficient) AND variation (e.g. standard deviation) or associated estimates of uncertainty (e.g. confidence intervals)
☒	☐	For null hypothesis testing, the test statistic (e.g. *F*, *t*, *r*) with confidence intervals, effect sizes, degrees of freedom and *P* value noted *Give P values as exact values whenever suitable.*
☐	☒	For Bayesian analysis, information on the choice of priors and Markov chain Monte Carlo settings
☒	☐	For hierarchical and complex designs, identification of the appropriate level for tests and full reporting of outcomes
☐	☒	Estimates of effect sizes (e.g. Cohen's *d*, Pearson's *r*), indicating how they were calculated
☐	☒	Clearly defined error bars *State explicitly what error bars represent (e.g. SD, SE, CI)*

Our web collection on statistics for biologists may be useful.

Software and code

Policy information about availability of computer code

Data collection	no software was used
Data analysis	featureCounts, Cutadapt, STAR, DESeq2, R 2.8 0, GraphPad, SAS statistic software, miRHub, Qiagen Ingenuity Pathway Analysis Version 01-13, RNAcofold 2.4.9

For manuscripts utilizing custom algorithms or software that are central to the research but not yet described in published literature, software must be made available to editors/reviewers upon request. We strongly encourage code deposition in a community repository (e g. GitHub). See the Nature Research guidelines for submitting code & software for further information.

Data

Policy information about availability of data

All manuscripts must include a data availability statement. This statement should provide the following information, where applicable:

- Accession codes, unique identifiers, or web links for publicly available datasets
- A list of figures that have associated raw data
- A description of any restrictions on data availability

The microarray dataset is available from Gene Expression Omnibus (GSE21545).
RNA-Seq data are deposited in the Gene Expression Omnibus under the accession number GSE97469.

Field-specific reporting

Please select the best fit for your research. If you are not sure, read the appropriate sections before making your selection.

☒ Life sciences ☐ Behavioural & social sciences ☐ Ecological, evolutionary & environmental sciences

For a reference copy of the document with all sections, see nature.com/authors/policies/ReportingSummary-flat.pdf

Life sciences study design

All studies must disclose on these points even when the disclosure is negative.

Sample size	No power calculation or selection of patients based on any other clinical criteria other than undergoing surgery was done for sample size; instead tissues were arrayed based on sample availability and RNA quality.
Data exclusions	No data was excluded.
Replication	All experiments were repeated 3-5 times and included positive and negative controls.
Randomization	For animal studies, groups were balanced and randomized based on serum lipoprotein profiles and body weight. The human studies were case controlled and thus were not randomized.
Blinding	For animal and human studies, investigators were unblinded to group allocations. Blinding was not necessary because these were case control studies involving the characterization of a new gene.

Reporting for specific materials, systems and methods

Materials & experimental systems

n/a	Involved in the study
☒	☐ Unique biological materials
☐	☒ Antibodies
☐	☒ Eukaryotic cell lines
☒	☐ Palaeontology
☐	☒ Animals and other organisms
☐	☒ Human research participants

Methods

n/a	Involved in the study
☒	☐ ChIP-seq
☒	☐ Flow cytometry
☒	☐ MRI-based neuroimaging

Antibodies

Antibodies used	LXRα antibody (Abcam, #ab41902) - 1:300; LXRβ antibody (Abcam, #ab56237) - 1:300; Isotype matched IgG (Abcam, #ab171870) - 1:1000; Rabbit anti-human EDC4 (Cell Signaling Technology, #2548) – 1:400; Goat anti-rabbit secondary antibodies (Life Technologies, #A-11011) – 1:1000; ABCA1 (Novus Biologicals, NB400-105) – 1:500 HSP90 (BD Biosciences, #610419) - 1:1000; Polyclonal anti-human apoA-1 (EMD Millipore, #178422); human AGO2 (Millipore, RIPAb+ #03-110); GFP (Roche Diagnostics, #118144600001) – 1:200; Isotype matched IgG control antibody (EMD Millipore, #CS200621) - 1:250
Validation	All antibodies were obtained from companies and tested before use for off target effects and efficiency LXRα antibody – Citeab com 6 publications for use in ChIP; LXRβ antibody - Citeab com 9 publications for use in ChIP; Isotype matched IgG - Abcam website, used in 31 publications for ChIP; Rabbit anti-human EDC4 – 3 publications on cell signaling website; goat anti-rabbit secondary antibodies - Citeab com 112 publications for use in immunofluorescence; ABCA1 - Citeab com 131 publications for use in western blotting; HSP90 – Citeab com 72 publications for use in western blotting; polyclonal anti-human apoA-1 - Citeab com 17 publications; human AGO2 - Citeab com 7 publications for immunoprecipitation; GFP – 10 publications on sigma website; Isotype matched IgG control antibody (EMD Millipore, #CS200621) - 7 publications on EMD website for IP

Eukaryotic cell lines

Policy information about cell lines

Cell line source(s)	HEK293T, HepG2 and THP-1 cell lines were obtained from American Type Tissue Collection.
Authentication	HEK293T, HepG2 and THP-1 cell lines were authenticated using standard American Type Tissue Collection methods including morphology check by microscope and growth curve analysis.
Mycoplasma contamination	HEK293T, HepG2 and THP-1 cell lines were tested monthly for mycoplasma contamination using the Sigma LookOut Mycoplasma PCR Detection Kit MP0035-1KT
Commonly misidentified lines (See ICLAC register)	No commonly misidentified cell lines were used.

Animals and other organisms

Policy information about studies involving animals; ARRIVE guidelines recommended for reporting animal research

Laboratory animals	African green monkeys Chlorocebus aethiops, male, mean 6 4 years, age range 5-10; Cynomolgus monkeys: Macaca fascicularis, male, mean 2 8 years, age range 2 5 – 3 1
Wild animals	The study did not involve wild animals.
Field-collected samples	The study did not involve samples collected from the field.

Human research participants

Policy information about studies involving human research participants

Population characteristics	Patients with established vascular disease in ongoing studies at NYULMC (NCT02106429 and NCT01897103) were studied. Patients undergoing surgery for stable or unstable carotid stenosis were studied. Mean age 69.5 years, 100 males and 27 females. Control samples were from undiseased macroscopically atherosclerosis free-arteries, iliac and one aorta obtained from organ donors without any current or history of cardiovascular disease. No biases were present for selecting samples.
Recruitment	- We identified patients with established vascular disease in ongoing studies (NCT02106429 and NCT01897103). Plasma samples were collected in accordance with the policies of New York University Langone Medical Center. All studies were approved by the NYULMC ethics committee. - The BiKE study is approved by the Ethical Committee of Northern Stockholm with following ethical permits: EPN DNr 95-276/277; DNr 02-146; DNr 02-147, DNr 2005/83-31; DNR 2009/512-31/2; 2012/619-32). The project is performed under the Swedish biobank regulations and prospective sampling is approved with informed consent procedure (DNr 2009/512-31/2). All samples were collected with informed consent from patients, organ donors or their guardians - Healthy liver tissue and serum samples were obtained from individuals undergoing liver surgery and experimental procedures were performed within the framework of the non-profit foundation HTCR Stiftung, including the informed patient's consent. This study was approved by the Ethics Committee of the Bavarian Medical Association (Bayerische Landesärztekammer) and the Ethics Committee of the Ludwig-Maximilians-University (LMU) Munich.